

TYPE IA SUPERNOVA: CALCULATIONS OF TURBULENT FLAMES USING THE LINEAR EDDY MODEL

S. E. WOOSLEY¹, A. R. KERSTEIN², V. SANKARAN², AND F. RÖPKE³

Draft version September 11, 2018

ABSTRACT

The nature of carbon burning flames in Type Ia supernovae is explored as they interact with Kolmogorov turbulence. One-dimensional calculations using the Linear Eddy Model of Kerstein (1991) elucidate three regimes of turbulent burning. In the simplest case, large scale turbulence folds and deforms thin laminar flamelets to produce a flame brush with a total burning rate given approximately by the speed of turbulent fluctuations on the integral scale, U_L . This is the regime where the supernova explosion begins and where most of its pre-detonation burning occurs. As the density declines, turbulence starts to tear the individual flamelets, making broader structures that move faster. For a brief time, these turbulent flamelets are still narrow compared to their spacing and the concept of a flame brush moving with an overall speed of U_L remains valid. However, the typical width of the individual flamelets, which is given by the condition that their turnover time equals their burning time, continues to increase as the density declines. Eventually, mixed regions almost as large as the integral scale itself are transiently formed. At that point, a transition to detonation can occur. The conditions for such a transition are explored numerically and it is estimated that the transition will occur for densities near $1 \times 10^7 \text{ g cm}^{-3}$, provided the turbulent speed on the integral scale exceeds about 15% sonic. An example calculation shows the details of a detonation actually developing.

Subject headings: supernovae: general; hydrodynamics, shock waves, turbulence

1. INTRODUCTION

Damköhler (1940) first discussed multiple regimes of turbulent chemical combustion and gave scaling relations for each. In modern terms, the two regimes can be distinguished by their Karlovitz number, Ka , (e.g., Peters 2000),

$$\frac{U_L}{S_{\text{lam}}} = Ka^{2/3} \left(\frac{L}{\delta_{\text{lam}}} \right)^{1/3}, \quad (1)$$

or equivalently,

$$Ka = \left(\frac{\delta_{\text{lam}}}{l_G} \right)^{1/2}. \quad (2)$$

Here U_L is the *rms* velocity of turbulent fluctuations on an integral scale, L ; S_{lam} is the laminar conductive speed; δ_{lam} is the width of the laminar flame; and l_G is the Gibson length. For isotropic Kolmogorov turbulence (assumed throughout this paper), the turbulent speed on the scale of the flame thickness is

$$v_{\text{turb}}(\delta_{\text{lam}}) = \left(\frac{\delta_{\text{lam}}}{L} \right)^{1/3} U_L, \quad (3)$$

and the Gibson scale, the size of the eddy that turns over in a (laminar) flame crossing time, is

$$l_G = \left(\frac{S_{\text{lam}}}{U_L} \right)^3 L. \quad (4)$$

For $Ka \lesssim 1$, individual laminar flames are moved around by the largest turbulent eddies while smaller eddies have little effect. The overall burning progresses

at a speed determined by turbulence properties and is independent of the burning rate on small scales. This regime has been extensively explored in the astrophysical context (Niemeyer 1995; Niemeyer & Hillebrandt 1995; Niemeyer & Woosley 1997) and its properties are reflected in the Munich group’s subgrid model for flame propagation (Schmidt et al. 2006a,b).

The condition $Ka \gg 1$, on the other hand, implies that turbulence can penetrate into the flame and transport heat, and possibly fuel, faster than laminar burning crosses a flame width. An equivalent condition is that the Gibson scale is much less than the flame thickness. This regime too has been discussed in the astrophysical literature (Khokhlov, Oran, & Wheeler 1997; Lisewski et al. 2000; Niemeyer & Woosley 1997; Niemeyer & Kerstein 1997). It is generally agreed that if spontaneous detonation is to occur, it requires $Ka > 1$ and probably $Ka > 10$ so that the burning region itself is disrupted, not just the preheat zone.

It is also known in the chemical combustion community (Kerstein 2001; Peters 1986, 2000) that the region $Ka \gg 1$ can be further divided based on the value of the Damköhler number, $Da = L/(U_L \tau_{\text{nuc}})$. Here τ_{nuc} is the characteristic burning time scale, appropriately modified by turbulence. For $Da < 1$, the eddy turnover time on the integral scale is short compared with the nuclear time; for $Da > 1$, it is longer. In the literature, the term “distributed reaction zone(s)” has been used with reference to the $Da < 1$ regime, the $Da > 1$ regime, or both lumped together (i.e., all flames with $Ka \gg 1$). Therefore we avoid this terminology, choosing instead to follow Peters (1986) in referring to $Da < 1$ as the “well-stirred reactor regime” (WSR regime), and to follow Kerstein (2001) in referring to $Da > 1$ as the “stirred flame regime” (SF regime).

In the WSR regime, there is only one flame. It has a width broader than the integral scale and a speed slower

arXiv:0811.3610v1 [astro-ph] 21 Nov 2008

¹ Department of Astronomy and Astrophysics, University of California, Santa Cruz, CA 95064; woosley@ucolick.org

² Combustion Research Facility, Sandia National Laboratory, Livermore, CA; arkerst@sandia.gov

³ Max Planck Institut für Astrophysik, Garching, Germany; fritz@mpa-Garching.mpg.de

than the turbulent speed on the integral scale. This sort of flame is similar to the usual laminar flame, except that the turbulent diffusion coefficient ($D_{\text{turb}} \sim U_L L$) now substitutes for conduction. Within the SF regime, on the other hand, there can be multiple burning regions, but the idea of a flame brush composed of individual flamelets with well-defined local properties is no longer valid. The overall burning continues with an average rate given by the turbulent speed on the integral scale, but the flamelets do not have a uniform width and their number and individual speeds are quite variable.

In this paper, we explore these three regimes of turbulent nuclear combustion, $Ka < 1$, WSR, and SF, in the context of a Type Ia supernova using a numerical tool, the Linear Eddy Model (§ 3.1). If a transition to detonation is to occur, we conclude that it must happen in the SF regime, specifically where $Da \sim 10$ and in the presence of a high degree of turbulence, $U_L \gtrsim 0.15 c_{\text{sound}}$. An example of a successful spontaneous transition to detonation is given.

2. SPECIAL CONDITIONS IN A TYPE IA SUPERNOVA

The conditions characterizing turbulent (nuclear) combustion in a Type Ia supernova are novel and have no direct analogue on earth. This makes the supernova an interesting environment for testing new physics, but it also means that our terrestrial intuition regarding flames can be misleading. For example, it is thought that laboratory flames in the $Ka \gg 1$ regime simply go out (Peters 2000) because they are unable to maintain their heat in the presence of so much turbulence. But the flame in a supernovae can never “go out” until the star comes apart and, in terms, of local flame variables, that takes a very long time. The relevant time scale is the hydrodynamic time scale for the whole star, ~ 1 s, not the shorter local turbulent time scale, U_L/L . Also the star is very large, $\gtrsim 10^8$ laminar flame thicknesses and 100 integral scales. Rare events have many opportunities for realization. There are also other conditions that are vastly different and, in some cases, make detonation more easily achievable.

2.1. High Reynolds Number

The Reynolds number in a Type Ia supernova is orders of magnitude greater than achieved thus far in any terrestrial experiment or in any numerical simulation. The source of viscosity is electron-ion interactions in a fully ionized plasma (Nandkumar & Pethick 1984)

$$\nu = \frac{1.9 \times 10^6}{Z} \left(\frac{(\rho_6/\mu_e)^{5/3}}{1 + 1.02(\rho_6/\mu_e)^{2/3}} \right) \frac{1}{I_2} \quad (5)$$

$$\sim 2 \times 10^6 \text{ gm cm}^{-1} \text{ s}^{-1}$$

for $Z = 7$, $\mu_e = 2$, $\rho_6 = 10$, and $I_2 = 0.5$. The Reynolds number is then

$$Re = \frac{\rho U_L L}{\nu} \sim 5 \times 10^{13}, \quad (6)$$

for $\rho = 10^7 \text{ g cm}^{-3}$, $U_L = 100 \text{ km s}^{-1}$, and $L = 10 \text{ km}$. This large value of Re implies a tiny Kolmogorov scale, much smaller than any laminar flame thickness under consideration here, and irresolvably small in most numerical simulations,

$$\eta = Re^{-3/4} L \sim 10^{-4} \text{ cm}. \quad (7)$$

Note also that this implies ten orders of magnitude in length scale where the turbulence is (assumed to be) Kolmogorov and isotropic with constant energy dissipation, U_L^3/L .

On earth, the Kolmogorov scale is usually not so small compared with the flame thickness. This makes achieving the SF and WSR regimes more difficult on earth, though certainly not impossible.

2.2. Temperature-Dependent Heat Capacity

The heat capacity in the supernova at a relevant density, $\rho \sim 10^7 \text{ g cm}^{-3}$, is due to a combination of semi-degenerate electrons, ions and radiation. Radiation is an important component of the heat capacity at these low densities and hence the heat capacity is a rapidly increasing function of the temperature. At a density of 10^7 g cm^{-3} , for 50% C and 50% O, the heat capacity at constant pressure is 3.5, 6.0, 9.0, 12.7, 18.2, and $27.3 \times 10^7 \text{ erg gm}^{-1} \text{ K}^{-1}$ for a temperature of 0.5, 1.0, 1.5, 2.0, 2.5, and $3.0 \times 10^9 \text{ K}$ respectively. The power of T upon which C_p depends varies from 0.70 to 2.70 in the same temperature range.

This means that when the fuel is cold, a small amount of burning raises the temperature a lot. Given the high power of temperature upon which the burning depends, burning just a little fuel dramatically shortens the nuclear time scale.

2.3. Temperature-Dependent Reaction Rate

The most important reaction rate in the regime where detonation might occur is $^{12}\text{C} + ^{12}\text{C}$. The rate for this reaction is proportional to $\rho X^2 (^{12}\text{C}) T^n$ with $n \sim 19 - 27$ for temperatures in the range $1 - 3 \times 10^9 \text{ K}$ (more sensitive at lower temperature). This high temperature sensitivity coupled with the temperature-dependent heat capacity means that once about half of the carbon has burned, the remaining increase in the temperature happens very rapidly. As we shall see later this leads to small but very rapid increases in the local pressure that can help initiate a detonation.

2.4. Strong Turbulence

As burning plumes of ash float due to the Rayleigh-Taylor instability, they create shear and turbulence on their boundaries. Since the plumes are large, the speed at which buoyancy balances drag is high. A speed of order 10 - 30% sonic is necessary to burn a large fraction of the star before it comes apart. Typical turbulent speeds on an integral scale of 10 km are about 150 km s^{-1} (Röpke 2007), but speeds as great as 1000 km s^{-1} may occasionally occur. The sound speed in the star at a density of 10^7 g cm^{-3} is 3500 km s^{-1} , so the fastest turbulence is not terribly subsonic. Fluctuations in burning rate do not have to accelerate the burning by orders of magnitude in order to make a detonation happen.

2.5. Large Lewis Number

The Lewis number, which is the ratio of thermal diffusivity to mass diffusivity, is very large in the supernova. The ionic diffusion coefficient for a carbon-oxygen plasma is (Bildsten & Hall 2001; Hansen et al. 1975)

$$D_{\text{ion}} = 3\omega_p \alpha^2 \Gamma^{-4/3} \sim 0.1 \text{ cm}^2 \text{ s}^{-1}, \quad (8)$$

where $\omega_p = (4\pi n_i(Ze)^2/Am_p)^{1/2}$ is the plasma frequency, $\alpha = (3/(4\pi n_i))^{1/3}$, with n_i , the ion density, and $\Gamma = (Ze)^2/\alpha kT$. The thermal diffusion coefficient is

$$D_{\text{rad}} = \frac{4acT^3}{3\rho^2 C_P \kappa} \sim 10^4. \quad (9)$$

Here representative conditions and opacities have been assumed: $T \approx 1 - 2 \times 10^9$ K, $\rho = 10^7$ g cm⁻³, and $\kappa \approx 0.02$ cm² gm⁻¹ (Timmes 2000). Combining these two equations, $Le = D_{\text{rad}}/D_{\text{ion}} \sim 10^5$.

Terrestrial Lewis numbers are close to unity. The large Lewis number in the star has an effect on the laminar speed (§ 4), but this dependence is greatly mitigated in the turbulent regime (§ 5.3) where the turbulent diffusion coefficient exceeds D_{rad} . In that case, the effective Lewis number approaches unity since both ions and heat are transported with equal efficiency by the turbulent eddies (Aspden et al. 2008).

3. THE LINEAR EDDY MODEL

3.1. The LEM Code

The range of scales that must be resolved to address the flame propagation problem in a Type Ia supernova is very large, $\sim 10^{-1} - 10^6$ cm even if the Kolmogorov scale is not resolved. This range exceeds the current or anticipated capabilities of 3D simulations, or even 2D simulations. This conundrum arises for many turbulent flow environments, and motivated the development of the Linear Eddy Model (LEM), a 1D simulation tool (Kerstein 1991).

LEM simulates the evolution of scalar properties on a 1D spatial domain. This can be interpreted as property profile evolution along a 1D line of sight through 3D turbulent flow. The 1D domain is treated as a closed system with respect to enforcement of conservation laws. In this and other respects, LEM is not fully consistent with the evolution observed along a line of sight, yet it captures the salient features and provides useful results.

The physical processes that are time advanced on the LEM domain are diffusive (e.g., Fickian) transport (in the present context representing species transport, radiation transport or subgrid turbulent transport), chemical (or nuclear) reactions, and turbulent eddy motions. For combustion applications, including the present application, LEM includes an equation of state, an energy equation, and thermal expansion, using a zero-Mach-number (constant-pressure) formulation (Smith & Menon 1997). The novelty of the LEM approach is the representation of eddy motions.

On a 1D domain, advection in the usual sense cannot reorder the fluid elements along the domain, hence cannot emulate the folding of material surfaces that is an essential feature of turbulent stirring. A model of eddy motions is introduced that is formulated to capture this folding effect and other properties of turbulent stirring. Namely, a turbulent eddy is represented as an instantaneous map, called the triplet map, that is applied to a designated interval of the 1D domain.

The triplet map is applied by first compressing all property profiles in the interval by a factor of three. The property profiles in the interval are then replaced by three side-by-side copies ('images') of the compressed profiles. The middle copy is then flipped.

This procedure preserves the continuity of spatial property profiles. It also leaves the total linear measure (model analog of volume) of fluid corresponding to a given state or set of states (based on the property values) unchanged. This is the 1D analog of the solenoidal condition. Flipping of the middle copy introduces fluid-element reordering analogous to the folding of material surfaces. The three-fold compression emulates gradient amplification by compressive strain. The dispersive effect of extensive strain is represented in LEM by the mapping of neighboring fluid elements to different images.

Computationally, the triplet map is implemented as a permutation of the cells of a uniform discretization of the 1D domain. This and other details of LEM are explained elsewhere (Kerstein 1991). Here, features relevant to what follows are described. Some symbols that are used have different meanings than in later sections.

An LEM simulation time advances processes other than advection until it is time to implement a triplet map. After the map, advancement of the other processes resumes until it is time for the next map.

Model inputs are the initial and boundary conditions, the transport coefficients and rate constants governing diffusive and chemical advancement, and parameters controlling the time sequence of triplet maps. Map size l is sampled from a probability density function (pdf) $f(l)$ that is designed to reproduce relevant features of the inertial-range turbulent cascade. One key feature is the turbulent diffusivity D_{turb} associated with maps of size $l < S$. The inertial-range scaling $D_{\text{turb}} \propto S^{4/3}$ is enforced. In Kerstein (1991), it is shown that this implies $f(l) = Al^{-8/3}$, where A is a normalization factor.

Map size l is restricted to the range $[\eta, L]$, where η and L are the model analogs of the Kolmogorov scale and the integral scale, respectively. Then as shown in the Appendix, the total turbulent diffusivity is given by $D_{\text{turb}} = \frac{1}{18}\Lambda A(L^{4/3} - \eta^{4/3})$, where Λ is the total frequency of maps of all sizes per unit domain length. Here, homogeneous turbulence is assumed, so none of the model parameters depend on location, and map location is sampled uniformly within the notionally infinite 1D domain.

The parameters η , L , and D_{turb} are model inputs and Λ is determined from them. D_{turb} is not typically known for turbulent flows, but rather is inferred from the relation $D_{\text{turb}} = U_L L/C$, where C is an empirical coefficient. Here, LEM results are compared to 3D simulations of turbulent premixed combustion for which U_L and L are known, but D_{turb} is not, so C must be specified in order to evaluate the LEM input parameter D_{turb} . Smith & Menon (1997) calibrated C by comparing LEM results for turbulent premixed methane-air combustion (using a simplified chemical mechanism) to turbulent burning velocity measurements. They chose the value $C = 15$ for some cases and $C = 3.5$ for others, reflecting the wide variation of turbulent burning velocity results obtained in different experiments.

The experimental set-ups did not correspond to the idealized case of flames freely propagating through stationary, homogeneous turbulence. Here, LEM results are compared to 3D simulation results more closely analogous to the LEM flow configuration. The C value inferred from this comparison is close to the lower of the

two C values reported by Smith and Menon.

3.2. Modifications for the SN Ia Problem

The standard (i.e., terrestrial chemical combustion) version of LEM was modified to use an equation of state, opacities, and a nuclear reaction network appropriate to the supernova. The equation of state (the ‘‘Helmholtz EOS’’; Timmes & Swesty 2000) included pressure and energy contributions from radiation, ions (treated as an ideal gas), and electrons and pairs of arbitrary speed and degeneracy. The opacity routine (Timmes 2000) included heat transport by radiative diffusion and conduction. Energy generation and composition changes were followed using a nuclear reaction network with 7 species: ${}^4\text{He}$, ${}^{12}\text{C}$, ${}^{16}\text{O}$, ${}^{20}\text{Ne}$, ${}^{24}\text{Mg}$, ${}^{28}\text{Si}$, and ${}^{56}\text{Ni}$ (though no appreciable ${}^{56}\text{Ni}$ was ever produced in this study). These species were connected together by a chain of (α, γ) reactions as well as the heavy ion reactions 3α , ${}^{12}\text{C} + {}^{12}\text{C}$, ${}^{16}\text{O} + {}^{16}\text{O}$, and ${}^{12}\text{C} + {}^{16}\text{O}$. Though it is an unpublished version written by the authors, the network was similar to that of Timmes et al. (2000). The network did not include electron screening corrections to the reaction rates which were, in general, small at the low densities considered here. Testing the fast 7 isotope network against a larger 19 isotope network that included screening and about 85 reactions (Weaver, Zimmerman, & Woosley 1978) showed that the small network gave an energy generation that was typically 20 - 40% smaller. Since this is equivalent to a small error in the temperature, the results of the 7 isotope, unscreened network were deemed sufficiently accurate.

The code was then checked and calibrated against several other studies of flame propagation. For simple laminar flames (§ 4), the turbulence parameter, C (§ 3.1), doesn’t enter. For turbulent flames in the flamelet regime, the default setting $C = 15$ was used (§ 5.1). However, for flames in the WSR regime (§ 5.3), good agreement with prior 3D studies required a smaller value of $C = 5$. This value is within the range anticipated from terrestrial experiments (§ 3.1) and was used for all calculations in the WSR and SF regimes (i.e., all studies with $\text{Ka} > 1$) unless otherwise noted. Future 3D studies, especially of the SF regime, are encouraged in order to gain better confidence and understanding of C for flames of this sort.

4. SINGLE LAMINAR FLAMES

In the absence of turbulence, a flame has a simple structure in which a self-similar profile of temperature and fuel concentration propagates into the fuel with a well-defined width and speed. Heat is transported by a combination of conduction and radiative diffusion, and this heat raises the temperature to the point where fuel burns on a diffusion time scale. Such flames are well understood (Landau & Lifshitz 1959), even in the supernova context (Timmes & Woosley 1992). In multiple dimensions, laminar flames may become deformed and take on a cusp-like appearance due to the Landau-Darrieus instability (Niemeyer & Hillebrandt 1995), but this instability does not lead to a major destabilization of the overall burning (Röpke et al. 2004), nor does it greatly affect the propagation speed (Bell et al. 2004a).

As a test of the LEM implementation and to provide a calibration point for more complex studies to follow,

the one-dimensional laminar speed was calculated for carbon-burning flames at a variety of densities for two initial carbon mass fractions, $X_{12}^0 = 0.50$ and 0.75 . The results are given in Table 1 and Fig. 1. The speed of the flame with carbon mass fraction 0.50 and density 10^7 g cm^{-3} was $3.2 \times 10^3 \text{ cm s}^{-1}$, in good agreement with the $3.5 \times 10^3 \text{ cm s}^{-1}$ found by Aspden et al. (2008), who used somewhat different nuclear physics. The ash temperatures for the two compositions considered here were also in good agreement with the values calculated by Woosley (2007). The flame speeds for other densities were in agreement with previous studies by Bell et al. (2004b), and Timmes & Woosley (1992).

In these calculations, heat was transported by conduction and radiation and the laminar scale was well resolved. Zoning for the case of 10^7 g cm^{-3} , $X_{12}^0 = 0.50$ was 0.0244 cm and the flame width, several cm. A recalculation of the flame speed with coarser grids gave essentially the same answer. For resolutions of 0.196 cm and 0.0978 cm the calculated flame speed was 3.2 and $3.1 \times 10^3 \text{ cm s}^{-1}$, respectively, indicating that our calculation and that of Aspden et al. (2008) were both converged and did not differ because of resolution.

Some dependence on Lewis Number was noted. Two calculations of the speed for $X_{12}^0 = 0.50$ and $\text{Le} = 100$ and $\text{Le} = 1000$ gave speeds of $3.0 \times 10^4 \text{ cm s}^{-1}$ and $3.2 \times 10^4 \text{ cm s}^{-1}$ respectively.

5. THREE REGIMES OF TURBULENT BURNING

5.1. Large Scale Turbulence and Flame Brushes (Flamelet Regime)

The interior of a Type Ia supernova is turbulent, first because of the convection that precedes the explosion, which gives a lower bound for $U_L \sim 50 - 100 \text{ km s}^{-1}$ (Kuhlen et al. 2006; Woosley et al. 2004), and second because of the Rayleigh-Taylor and Kelvin-Helmholtz instabilities associated with the flame itself (Hillebrandt & Niemeyer 2000). Because these speeds are so much greater than the laminar speed (Table 1), especially at low density, it is expected that turbulence has a major effect on flame propagation. Initially, however, the flame is very thin compared to the Gibson length and is just carried around by the eddies (Damköhler 1940). Overall the burning rate is independent of the speed of each little flamelet, and is governed instead by the speed of the largest turbulent eddies. This is Damköhler’s ‘‘large scale turbulence’’ limit.

To illustrate burning in this regime, we considered a laminar flame similar to that in Fig. 1 with a carbon mass fraction of 0.75 and a fuel density $1.0 \times 10^7 \text{ g cm}^{-3}$, but embedded in a turbulent background with characteristic speed 400 m s^{-1} on an integral scale of 10 m . On this length scale in a supernova, one would actually expect much larger turbulent speeds, 10 to 100 km s^{-1} , cascading down from still higher values on larger scales. For the time being such large, highly turbulent regimes with narrow flames remain out of computational reach, even in 1D. Conditions chosen here were thus artificial, but illustrative. The Gibson scale here (eq. 4) is 21 cm , considerably larger than the laminar flame width, which is $\sim 1 \text{ cm}$ (Fig. 1), but still about still 50 times less than the integral scale. The results are given in Fig. 2. Sometimes only a single flame was observed, but at the particular moment sampled here, there were eleven (counting the

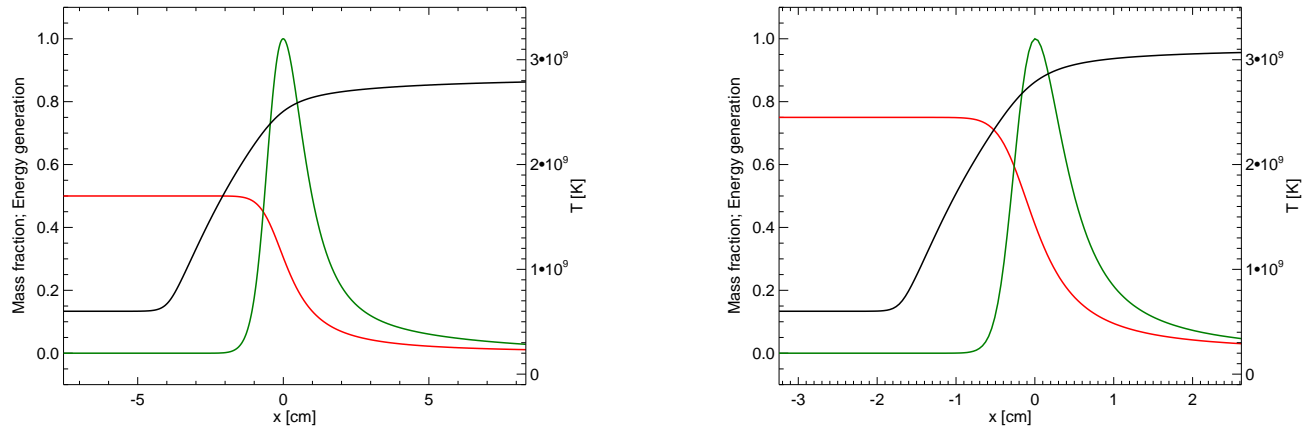


FIG. 1.— Laminar flame structure for initial carbon mass fractions of 0.50 (left frame) and 0.75 (right frame) and a density of $1.0 \times 10^7 \text{ g cm}^{-3}$. Carbon mass fraction is given in red and the temperature, in units of 10^9 K , is in black. The energy generation (green) has been normalized to a maximum value of $7.47 \times 10^{20} \text{ erg g}^{-1} \text{ s}^{-1}$ ($X_{12}^0 = 0.50$) and $8.40 \times 10^{21} \text{ erg g}^{-1} \text{ s}^{-1}$ ($X_{12}^0 = 0.75$). The flame is propagating to the left with a speed of $3.2 \times 10^3 \text{ cm s}^{-1}$ ($X_{12}^0 = 0.50$) and $1.1 \times 10^4 \text{ cm s}^{-1}$ ($X_{12}^0 = 0.75$). The assumed Lewis Number in both cases was 1000. These calculations with the LEM code used 2048 zones and show its ability to resolve and physically calculate laminar flames where radiation transport is dominant.

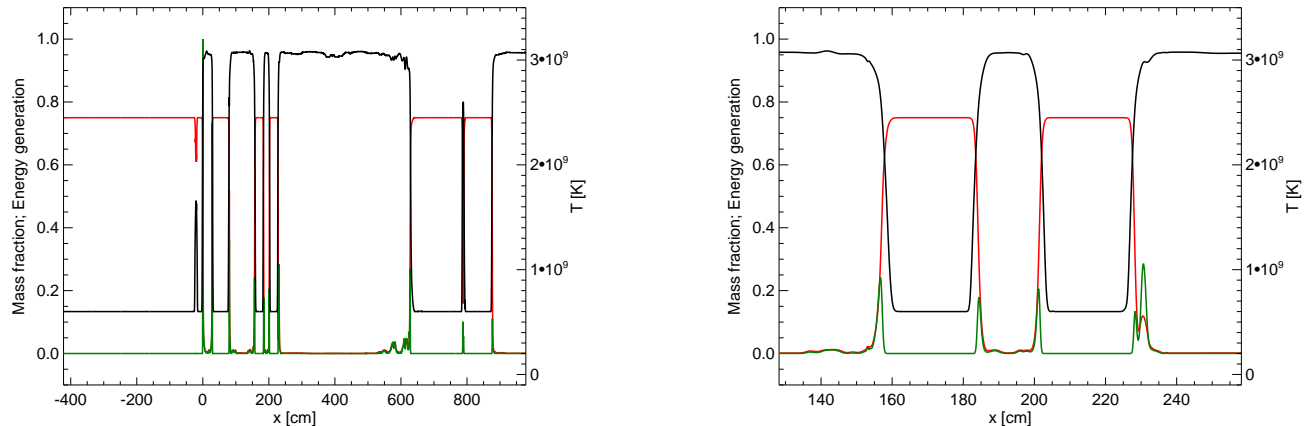


FIG. 2.— Multiple laminar flames for a carbon mass fraction of 0.75, density, $1.0 \times 10^7 \text{ g cm}^{-3}$, integral length scale, 10 m, and turbulent speed on that scale, 400 m s^{-1} . The left frame shows the entire flame brush, while the right frame shows greater detail for a few of the flamelets. The entire collection of flamelets is moving to the left at an average rate of 500 m s^{-1} (see Fig. 3). The time here is 0.015 s into the calculation and the instantaneous rate of burning corresponds to a speed of 980 m s^{-1} . This calculation with the LEM code used 40000 zones and $Le = 100$.

small blip of entrained ash at 800 cm).

Fig. 3 shows the overall propagation speed of the flame brush. Here, as in the rest of the paper, the burning “speed” is defined by an integral over the grid of the burning rate,

$$v_f = \frac{\int S_{\text{nuc}} dx}{q}, \quad (10)$$

where S_{nuc} is the nuclear energy generation rate on the grid ($\text{erg g}^{-1} \text{ s}^{-1}$), and q is the energy released by burning a gram of fuel. For fuel with 50% carbon, q is $3.2 \times 10^{17} \text{ erg g}^{-1}$ and for 75% carbon it is $4.5 \times 10^{17} \text{ erg g}^{-1}$.

For the case shown in Fig. 3, the average burning speed is 500 m s^{-1} , close to the turbulent *rms* speed on the integral scale, 400 m s^{-1} . In LEM, one expects for the flamelet regime that $v_{\text{turb}} = 18 D_{\text{turb}}/L$ (see Appendix).

Combining this with $D_{\text{turb}} = U_L L/C$ (§ 3.1) and using the same value for C as the simulation ($C = 15$), one has $v_{\text{turb}} = (18/15) U_L$, which is excellent agreement.

Fig. 3 also shows that the burning rate is far from regular. Speeds over three times the average are sometimes seen. At other times, the flame briefly almost goes out. A similar behavior would be expected in the actual supernova early on when the density is higher and the turbulent speed is not that much greater than the laminar one. Then, as here, there would be just a few flames within the integral scale and the burning rate would be highly irregular. For example, at a density of 10^9 g cm^{-3} with a carbon mass fraction of 0.50, the laminar flame speed is 36 km s^{-1} (Timmes & Woosley 1992) and the ratio $L/l_{\text{Gib}} \sim (U_L/S_{\text{lam}})^3$ is, for $U_L = 130 \text{ km s}^{-1}$, also about 50. The difference at these high densities is that

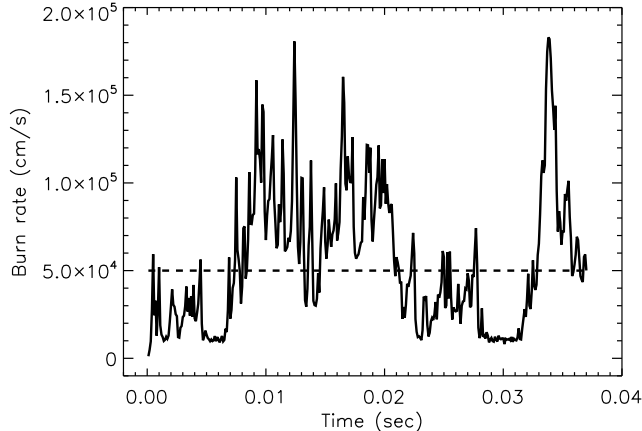


FIG. 3.— Speed of the flame brush as a function of time for the same calculation shown in Fig. 2. The speed, as measured by the overall energy generation on the grid, is highly variable ranging from a lower bound given by the laminar speed of a single flamelet ($1.1 \times 10^4 \text{ cm s}^{-1}$) to several times the mean value. The dashed line indicates the average during the time interval studied, $5.5 \times 10^4 \text{ cm s}^{-1}$, which is close to the *rms* turbulent speed on the integral scale, $4 \times 10^4 \text{ cm s}^{-1}$. The turnover time on the integral scale is 0.025 s and one sees the effect of the occasional large eddy in accelerating the burning.

the flame would be irresolvably small, even in the present version of LEM, for a calculation that carried the entire integral scale.

5.2. Transition to Stirred Flames

The flames at such high density are individually very thin and the laminar speed far below sonic, so detonation at early times is avoided. As the density declines, the Gibson length shrinks and the flame brush contains an increasingly large number of flamelets. Just before entering the SF regime in the supernova, there are roughly a thousand flamelets within the flame brush ($U_L \sim 100 \text{ km s}^{-1}$; $S_{\text{lam}} \sim 100 \text{ m s}^{-1}$). The statistical variations in overall speed are therefore small.

As the density in the star declines below several times 10^7 g cm^{-3} , the Gibson length becomes less than the laminar flame width and the transport of fuel and heat by turbulent advection starts to become important on the scale of the flame. By the time the density reaches $1.0 \times 10^7 \text{ g cm}^{-3}$, for typical turbulent speeds, not only is the preheat region of the flame being mixed by turbulence, but the burning zone itself has been disrupted and combustion has a qualitatively different character (Aspden et al. 2008; Peters 2000). In the star, this transition is brought about by the slowing and thickening of the laminar flame with decreasing density in a background of turbulence with nearly constant energy dissipation rate and integral length scale.

5.3. The Well-Stirred Reactor (WSR Regime)

Before discussing the stirred flame regime further though (§ 5.4), it is helpful to consider a limiting case where the turbulence thickens a single flame to a dimension greater than the integral scale, i.e., $\delta_{\text{turb}} > l$, where l is some integral scale to be varied subject to the condition $v'^3(l)/l = \epsilon = \text{constant}$, where v' is the velocity on

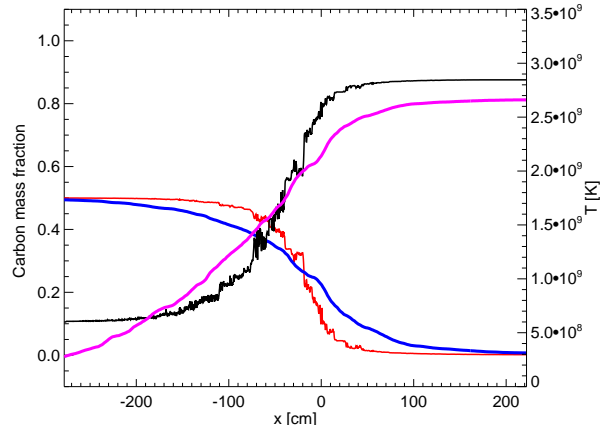


FIG. 4.— Comparison of carbon mass fraction and temperature for two flames calculated at a density of 10^7 g cm^{-3} , integral scale, $l = 15 \text{ cm}$, and turbulent speed, $2.45 \times 10^5 \text{ cm s}^{-1}$. The purple and blue curves are the average temperature and carbon mass fraction from the 3D study of Aspden et al. (2008). The black and red curves are from the corresponding study using LEM and $C = 5$ (Table 2). The speed of the flame calculated in 3D was $1.8 \times 10^4 \text{ cm s}^{-1}$. With LEM it was $1.5 \times 10^4 \text{ cm s}^{-1}$, about five times the laminar flame speed for these conditions. The flame widths calculated in the two studies are quite similar. Differences in the temperature are attributable, in part, to the different fuel temperature employed in the two studies - $1 \times 10^8 \text{ K}$ for the 3D study and $6 \times 10^8 \text{ K}$ for the LEM study and the smaller network used for the 3D study (see text).

the integral scale, l . While probably not realized in the supernova because of the large integral scale, this is the regime most easily accessible to multi-dimensional simulations and corresponds to what is commonly meant by the “well-stirred reactor” (e.g., Fig. 7 of Peters 1986). The solutions here also obey scaling relations predicted by Damköhler (1940).

5.3.1. An example compared with previous 3D simulations

Aspden et al. (2008) recently carried out 3D simulations of flame propagation in the WSR regime for a density and composition appropriate to Type Ia supernovae. We focus here on their calculation at 10^7 g cm^{-3} , $X_{12}^0 = 0.50$, and $\epsilon = U_L^3/L = 10^{15} \text{ erg g s}^{-1}$. Figures 4, 5, 6, and Table 2 show the results for an LEM calculation at the same values of integral scale, $l = 15 \text{ cm}$, and $v'(l) = 2.47 \text{ km s}^{-1}$ that they employed. A single broad flame propagates at a steady speed about 5 times faster than the laminar value. The width of the flame, as measured by the full width at half maximum of the energy generation curve is about 50 cm, or 20 times the laminar width (Fig. 1).

The most noticeable differences with the 3D calculation (Fig. 4) are a consequence of differing assumptions regarding the background (fuel) temperature in the supernova. Aspden et al. used $1 \times 10^8 \text{ K}$; here we use $6 \times 10^8 \text{ K}$. The lower temperature would characterize a region of low turbulence following some expansion prior to a detonation transition. The latter is characteristic of the convection zone in the supernova at the time of runaway. For a non-turbulent medium, the former is more physical. However, anticipating that we will be interested here in turbulent energies $U_L^3/L \sim 10^{17} - 10^{18} \text{ erg}$

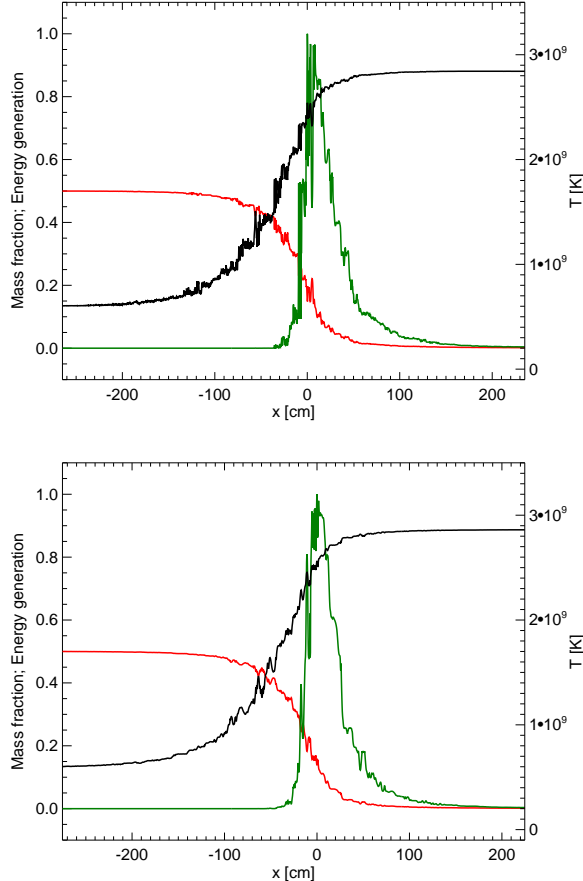


FIG. 5.— Two recomputations of the turbulently broadened flame in Fig. 4. Both calculations used the LEM code with a zoning of 2048 zones ($\Delta x = 0.147$ cm). The maximum energy generation in both plots is normalized to 2.3×10^{20} erg g^{-1} s^{-1} . The calculation in the first frame used a diffusive energy transport coefficient based on radiation and conduction. The one in the second frame, virtually identical in result, used the subgrid model discussed in the text.

g^{-1} s^{-1} and that at least a few turnovers on the integral scale are expected prior to a detonation, the latter is also a reasonable assumption. For $U_L \sim 10^8$ cm s^{-1} and $L = 10$ km, 10^{16} erg g^{-1} would be deposited in one turnover time. At a density of 10^7 g cm^{-3} , this corresponds to a temperature increase from 1×10^8 K (or essentially zero) to 6×10^8 K. Because of the temperature sensitivity of the heat capacity (§ 2.2), we expect our results to be insensitive to the assumed fuel temperature. However we do note that, if a fuel temperature of 1×10^8 is assumed in LEM, better agreement with the width is obtained than in Fig. 4, but the best value of C is lowered to $C = 2$.

While lower values of C are actually more favorable to detonation, we prefer to use the larger value because it is more consistent with the range seen in terrestrial experiments (§ 3.1) and because a hotter fuel temperature is both physically justifiable and more stable numerically.

For the calculation shown in the first frame of Fig. 5, energy transport by conduction and radiative diffusion was included, just as in the laminar flame cases, and zoning was sufficient to resolve a laminar flame had one

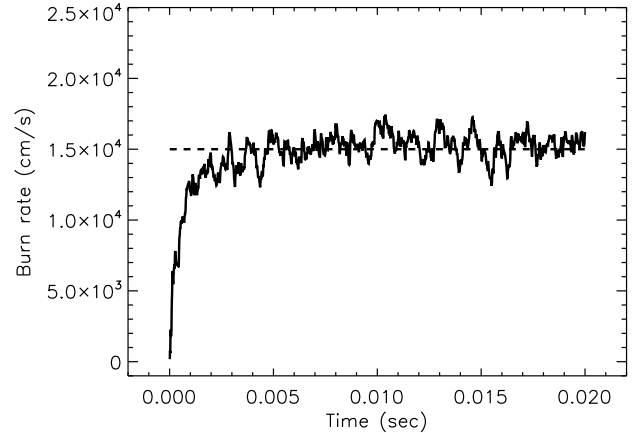


FIG. 6.— Speed of the turbulently broadened flame shown in Fig. 5 as a function of time. The turnover time on the integral scale is 6.1×10^{-5} s. It takes many turnover times to reach the terminal speed, but then that speed is maintained rather precisely. The dashed line shows the average speed, 1.5×10^4 cm s^{-1} , or 5 times the laminar value.

been present. However, the transport here is really dominated by the turbulence. The radiative diffusion coefficient (eq. 9) varies from 730 cm 2 s^{-1} in the fuel to 1.8×10^4 cm 2 s^{-1} in the ash while the turbulent diffusion coefficient (§ 3.1; $D_{\text{turb}} = v'l/C$ with $v' = 2.47$ km s^{-1} , $l = 15$ cm, and $C = 5$) is 7.4×10^5 cm 2 s^{-1} .

Fig. 7 shows the distribution of carbon with temperature in the case of a laminar flame (Fig. 1) and the turbulent flame (Fig. 5). Both plots show a single-valued, monotonic relation. For the laminar flame this is not surprising. At each temperature in the self-similar front there is a unique carbon abundance. When eddies, coupled with diffusion move heat and carbon around in a way that, in LEM at least, is discontinuous, the result is perhaps more surprising. It is also important that the curves are substantially different in the two cases.

The curve for the turbulent case in Fig. 5 is what one would result were carbon to burn at constant pressure *with no transport whatsoever* (Aspden et al. 2008). This means the process that is transporting heat is transporting composition with equal efficiency, i.e., the effective Lewis number is one. One expects this sort of behavior when turbulence is dominating in the transport of both. The Lewis number in the calculation was still 1000, but small scale eddies kept the mixture so well stirred that even a small amount of ionic diffusion at the grid scale gave the same result as if $Le = 1$. In fact, the actual turbulent transport would have been even more efficient had the resolution been higher. Recall that the Kolmogorov scale is not resolved here.

5.3.2. A subgrid model for turbulent transport

If the turbulent diffusion coefficient, $D_{\text{turb}} \sim v'l$, is so much greater than conduction and radiation, then the results should be independent of D_{rad} . The second frame of Fig. 5 shows that this is indeed the case. Here the calculation sets conduction and radiative transport to zero, but instead uses a diffusion coefficient coupling individ-

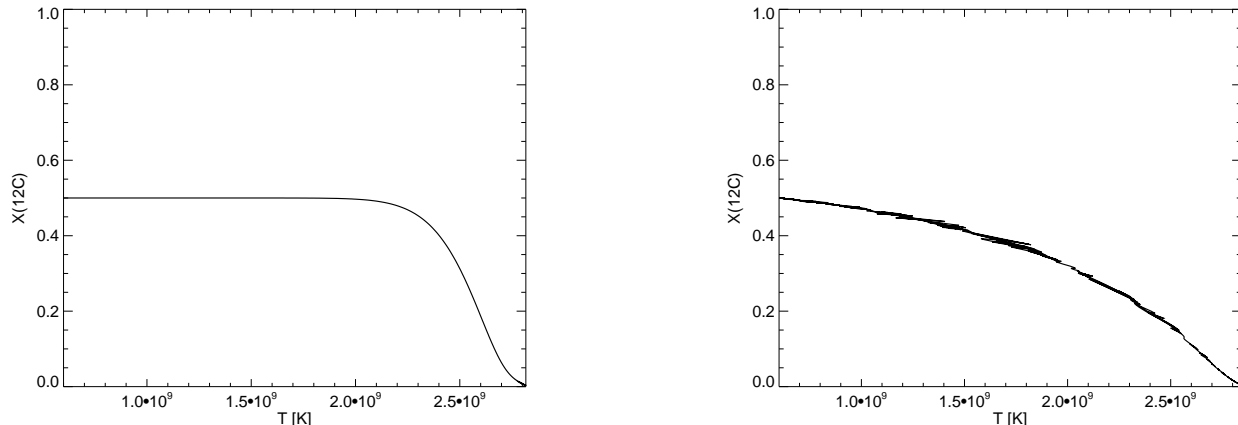


FIG. 7.— Carbon mass fraction as a function of temperature for all grid points for the calculation of the laminar flame (left; see also Fig. 1) and the turbulently broadened flame (right; see also Fig. 5). The initial density and carbon mass fraction in both cases were $X_{12}^0 = 0.5$ and $1.0 \times 10^7 \text{ g cm}^{-3}$. Burning in the laminar flame occurs chiefly at a higher carbon mass fraction due to preheating by radiation. Burning in the turbulent flame occurs as hot fuel and cold ash are mixed with negligible radiation transport. Because burning a certain fraction of carbon releases a certain amount of energy and, at constant pressure, gives a unique temperature, all points lie on a well-defined line. A mixture of radiation transport and advection would have given points in between these two lines (see also Aspden et al. (2008)).

ual zones of

$$D_{\text{SG}} = v(\Delta x) \Delta x \frac{15}{C} \quad (11)$$

where Δx is the grid resolution (constant in this paper), and

$$v(\Delta x) = \left(\frac{\Delta x}{l}\right)^3 v'. \quad (12)$$

The subgrid diffusion coefficient D_{SG} represents the mixing effects of unresolved eddies smaller than the grid scale. The results for $C = 5$ are identical.

The exact value of D_{SG} is not very important so long as it is derived from a length scale that is very much less than the (turbulently broadened) flame thickness. There is a characteristic eddy size that is chiefly responsible for the diffusion (Appendix A) and so long as that scale is well resolved, the results are similar. However there is a choice for D_{SG} that works best as the resolution becomes coarser. Fig. 8 shows that a diffusion coefficient derived from the turbulent speed on the grid scale has much better scaling properties than one based on e.g., $6\Delta x$, even though the smallest eddy in LEM is $6\Delta x$. The figure also shows that the diffusive properties of a temperature discontinuity remain unaltered as the resolution is decreased by a factor of 50.

5.3.3. The effect of increasing the integral scale

Encouraged by these results, which imply that one need not resolve the laminar scale in this regime in order to obtain accurate results, we proceeded to explore flame properties for a large range of l consistent with the condition $\epsilon_t = v'^3/l = 10^{15} \text{ erg g}^{-1} \text{ s}^{-1}$ (Table 2).

In general, the speed of a flame propagated by diffusion should obey the scaling relation

$$v_f \sim \sqrt{\frac{D}{\tau_{\text{nuc}}}}. \quad (13)$$

where $D_{\text{turb}} \sim v'l$. Fig. 9 shows the effect on the flame of increasing l at constant turbulent energy dissipation

ϵ , mass density, and carbon mass fraction. For awhile, the profiles follow the scaling implied by eq. 13. If the burning time is independent of l ,

$$\begin{aligned} v_{\text{turb}} &\propto (v'l)^{1/2} \propto l^{2/3}, \\ \delta_{\text{turb}} &\propto v_{\text{turb}} \propto l^{2/3}. \end{aligned} \quad (14)$$

For given, l , the flame speed also remains roughly steady.

However, this scaling also predicts its own breakdown. Since v_{turb} increases as $l^{2/3}$ while v' only increases as $l^{1/3}$ there must be a critical integral scale λ for which the two become equal. λ is determined by the relation $\lambda/v' = \tau_{\text{nuc}}$, where v' is the velocity fluctuation at scale λ . Rewriting this as $\lambda = (v'^3 \tau_{\text{nuc}}^3 / \epsilon)^{1/2}$ gives

$$\lambda = (\epsilon \tau_{\text{nuc}}^3)^{1/2}. \quad (15)$$

At $l = \lambda$, the flame width and integral scale are the same and the burning speed is approximately equal to the turbulent speed on that scale (Kerstein 2001; Woosley 2007). This is also the size of an eddy that burns in one turnover time. The quantity, $\epsilon = U_L^3/L$, is a constant by assumption. Approximate values of λ have been tabulated for various densities, turbulent energies and carbon mass fractions by Woosley (2007). Better values for the cases considered here can be inferred from the data in Table 2 which uses our reaction network. Once $l > \lambda$, the flamelets no longer has the appearance of a diffusively broadened structure, though the individual flamelets can occasionally coalesce into larger structures. This is the SF regime of the next section. As Fig. 10 and Fig. 11 show, the flame structure and speed both become highly variable as the integral scale approaches this value.

5.3.4. The nuclear time scale in the WSR regime

Burning in the WSR, $l < \lambda$, produces flames that, for a given constant density and fuel composition, have a well-defined nuclear time scale, τ_{nuc} . Fig. 12 shows the temperature, and nuclear time scale as function of

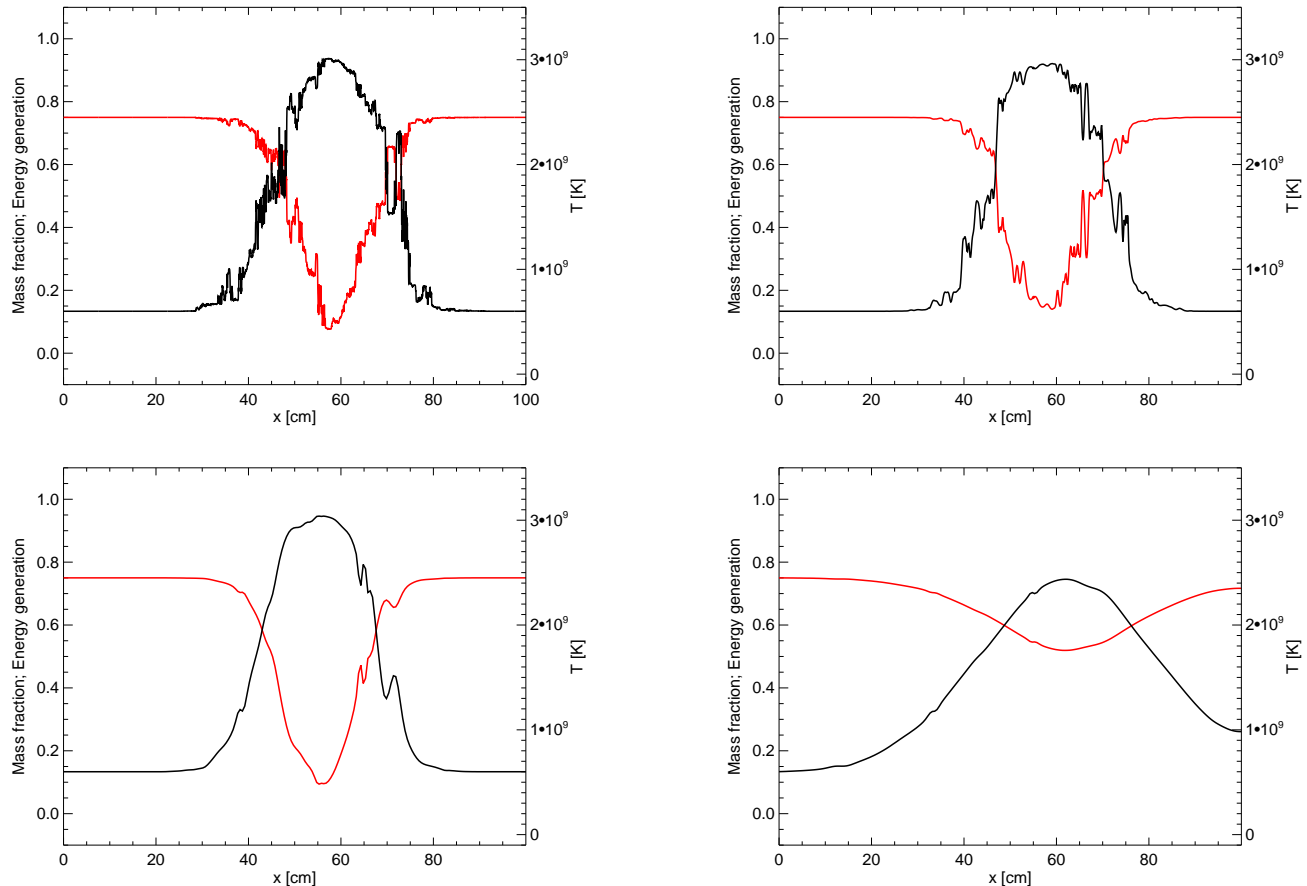


FIG. 8.— Resolution study of the subgrid model. Nuclear burning and conduction were turned off so that all transport was by turbulent eddies. Turbulence with a speed of 10 km s^{-1} was assumed on an integral scale of 5 cm . An island of ash 20 cm wide and initially centered at 50 cm was inserted in a background of fuel. The ensuing diffusive spreading was calculated using a grid of $10,000$ (first frame), 1000 (second frame), and 200 (third frame) zones. The extent to which the fuel diffuses after $5 \times 10^{-5} \text{ s}$ is very similar in all three runs. Larger subgrid diffusion coefficients on the other hand gave a resolution-dependent spreading that was more extensive for lower resolution. The fourth frame shows the result for $D_{\text{turb}} = v(6\Delta x)6\Delta x$ instead of $D_{\text{turb}} = v(\Delta x)\Delta x$ (see text). In that case, the image for 10000 zones (not shown) is virtually unchanged. (Note that the grid moves to keep the point $2 \times 10^9 \text{ K}$ centered.)

carbon mass fraction in the fuel for two initial carbon concentrations (50% and 75% by mass) and fuel density 10^7 g cm^{-3} . The burning is assumed to be isobaric and two time scales are computed. One time scale reflects the instantaneous rate of carbon consumption, $\tau = X_{12}/(dX_{12}/dt)$ (the dash-dotted line). More relevant to the flame speed, however, is the *induction* time scale, which is the time required to consume most of the remaining fuel. In a situation where burning increases the temperature, and therefore the reaction rate, the induction time can be much shorter than the instantaneous burning time scale (defined by the current abundance divided by the current burning rate). Dividing the turbulent flame width by the turbulent flame speed for those cases in Table 2 where both quantities are well defined gives an approximately constant value $\tau_{\text{nuc}} \approx 0.003 \text{ s}$ for $\epsilon = 10^{15} \text{ erg g}^{-1} \text{ s}^{-1}$ and $X_{12}^0 = 0.50$. This corresponds to a carbon mass fraction in Fig. 12 of $X_{12} \approx 0.20$ where the energy generation is about $1/e$ of its maximum.

Defining τ_{nuc} in this fashion as the induction time scale from the point where the energy generation reaches $1/e$ of its eventual maximum allows the computation of

$\lambda = (\epsilon\tau_{\text{nuc}}^3)^{1/2}$. For the case of carbon mass fraction in the fuel = 75%, the induction time scale was calculated based on a starting carbon mass fraction of 37%. The values of λ so determined are given in Table 3. These values are about a factor of two less than given in Woosley (2007) because they refer to a time scale derived from the width of the energy generating region. If one instead uses the larger width based upon temperature or carbon mass fraction, the derived values for λ are about twice as large, consistent with Woosley (2007).

5.4. Stirred Flames (SF Regime)

The stirred flame (SF) regime, which is characterized by $\text{Ka} \gg 1$ and $\text{Da} = L/(U_L\tau) = (L/\lambda)^{2/3} > 1$, is the most complex of the three regimes of turbulent burning. In this case, there is no well-determined scale for the flame width. Structures of size $\sim \lambda$ persist to some extent, but since the flame experiences a new eddy of length λ , in approximately the same time it takes to burn a distance λ , it is subject to continual disruption. At times there may be almost no burning; at others, nearly simultaneous burning happens on scales much larger than λ .

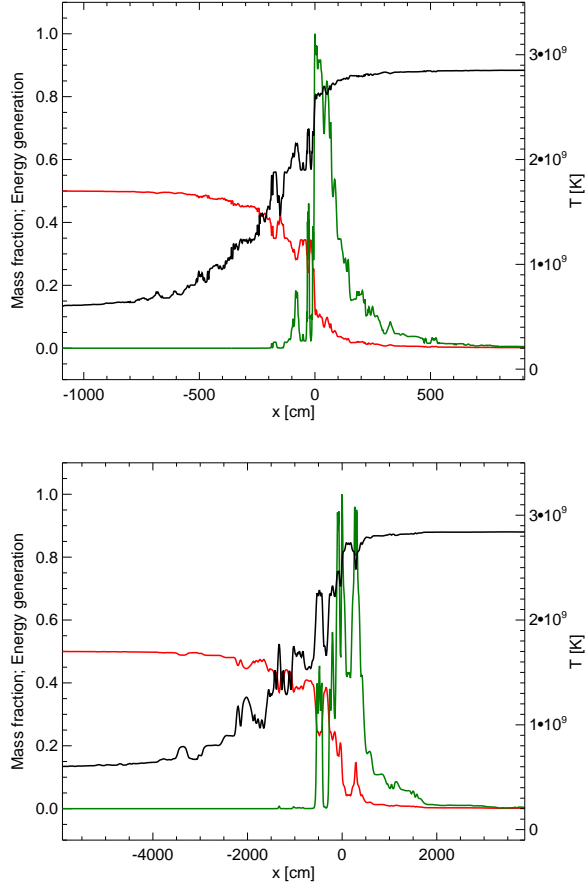


FIG. 9.— Flames for larger integral scales than Fig. 5, but still in the WSR regime. The integral scales are 120 cm (first frame) and 960 cm (second frame), and the corresponding *rms* turbulent speeds on those scales, 4.93 km s^{-1} and 9.86 km s^{-1} . The average propagation speeds are 0.61 km s^{-1} and 2.3 km s^{-1} . Note that both the flame speeds and widths scale as $l^{2/3}$ in this regime, both in this figure and as compared with Fig. 5. In the flame with the larger integral scale (right frame), one begins to see some structure in the flame and small “ledges” of mixture with nearly constant fuel abundance and temperature (§ 5.4.3).

The fact that the flame has no persistent steady state also reflects a poorly defined nuclear time scale. Each temperature has a different burning time scale and thus the characteristic widths of mixtures prepared by the turbulence is very temperature sensitive. Cooler mixtures have larger length scales. In general though, the average time scales are longer and the flame structures larger than expected from our studies of the WSR.

Because of the large integral scale in the supernova, the SF regime is encountered as soon as the Karlovitz Number exceeds about 10. The Damköhler number at that point is already much greater than unity and the WSR regime ($\text{Da} < 1$) is encountered much later, if ever.

5.4.1. The transition from the flamelet to the SF regime

Just before the laminar flame is disrupted at $\text{Ka} \sim 10$, there are $\sim U_L/S_{\text{lam}}$ flame surfaces folded in the flame brush. The average spacing between these flamelets is $d \sim (L/U_L)S_{\text{lam}}$ (Table 3) and the thickness of each is δ_{lam} . A short time later, as Ka continues to increase,

these flamelets are smeared out to make a smaller number of broader, faster structures with characteristic average thickness λ . Their number then is $\sim \sqrt{\text{Da}} = (L/\lambda)^{1/3}$, and their spacing is $\sim L/\sqrt{\text{Da}} = L^{2/3}\lambda^{1/3}$. So long as $\text{Da} \gg 1$, as it is at the transition, the new broadened structures will, on the average, still be separated by distances much greater than their size and will not coalesce into one large mixture.

The quantity λ (eq. 15) that plays a such a critical role in this discussion can be thought of as a generalization of the Gibson length (eq. 4). For the flamelet regime, the Gibson scale is the size of the eddy that would be crossed by a laminar flame with speed S_{lam} on an eddy turnover time. It is smaller for larger turbulent energy. The quantity λ , on the other hand, is also the size of an eddy that turns over on a nuclear time scale, but its size depends only on turbulence properties, not the radiative diffusion that sets S_{lam} . It is larger for larger turbulent energy. As the supernova expands, the Gibson scale shrinks as S_{lam} declines. Eventually when $\text{Ka} = 1$, $l_G = \delta_{\text{lam}}$, but except for differences due to a changing nuclear time scale (§ 5.3.3), at $\text{Ka} = 1$, λ is also approximately equal to l_G and δ_{lam} . Thereafter, as the density decreases more, l_G ceases to have much meaning since laminar flame speeds are no longer relevant. The new relevant scale, $\lambda = (\epsilon\tau^3)^{1/2}$, on the other hand, grows rapidly at lower density due to the increasing nuclear time scale.

What this means is that the transition from laminar burning to the SF regime is probably smooth and uneventful. Flamelets will grow gradually in speed and width as the density declines, not discontinuously. Because the nuclear time, and thus λ , lack precise definitions in the SF regime, and because of intermittency, one cannot completely rule out large scale transient mixing at the laminar-SF transition, especially if the turbulent energy is very large, but a detonation here seems unlikely. If it did happen at such high density, a very bright supernova would result due to the near complete incineration of the star.

5.4.2. Complex structure

As the density continues to decrease, λ increases and there are fewer, thicker, faster turbulent flamelets in the flame brush (Fig. 10 and Fig. 11). The limit of one flame of size $\lambda = L$ is reached when $\text{Da} = 1$. This is the condition suggested by Woosley (2007) as likely for detonation. The present study shows, however, that mixed regions larger than λ can exist transiently even for $\text{Da} \gg 1$. Since the critical mass for detonation decreases rapidly with increasing density, this makes detonation easier.

Consider the case of 50% carbon, a turbulent dissipation rate of $10^{15} \text{ erg g}^{-1} \text{ s}^{-1}$, density 10^7 g cm^{-3} , and integral scale $l = 4.92 \text{ km}$ (Table 2). For these conditions, $\lambda = 64 \text{ m}$ (Table 3) and $\text{Ka} = (4.92 \times 10^5 / 6.4 \times 10^3)^{2/3} = 18$. The average number of flame surfaces is $\sqrt{\text{Ka}} \sim 4$. Fig. 13 shows that mixed regions as big as L (and much bigger than λ) occasionally exist. The extent of mixing and hence the flame speed is highly variable (Fig. 11). Most of the time, less mixing is seen than in Fig. 13 and only a few disjoint regions of burning are present, but structures like these can exist for an eddy turnover time

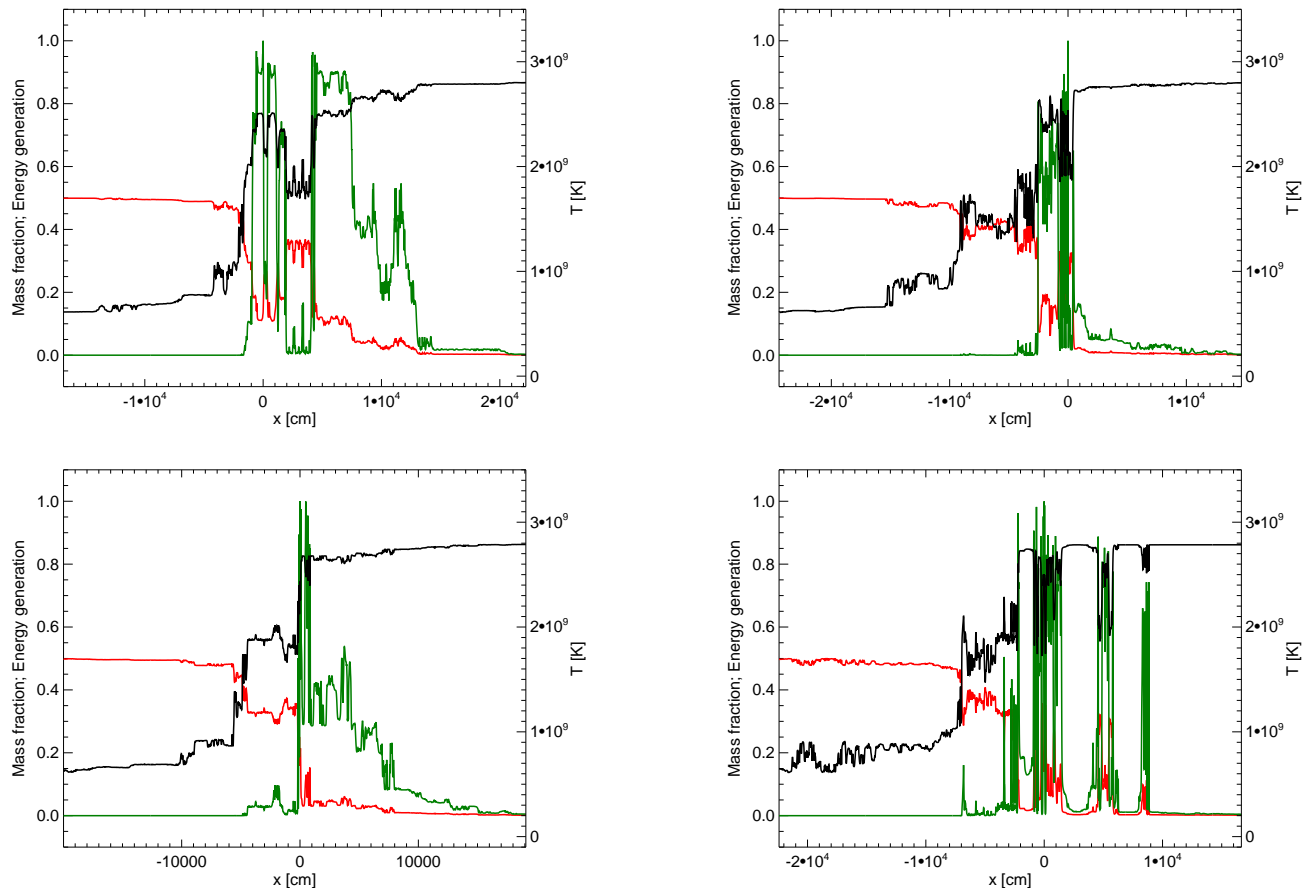


FIG. 10.— A turbulent flame calculated for a still larger integral scale than in Fig. 9 and sampled at four different times. The density and carbon mass fraction continue to be $1.0 \times 10^7 \text{ g cm}^{-3}$ and $X_{12}^0 = 0.50$, and $\epsilon = 10^{15} \text{ erg g}^{-1} \text{ s}^{-1}$. The integral scale here is 76.8 m and the flame’s average speed is 8.3 km s^{-1} compared with an rms turbulent speed on the integral scale of 19.7 km s^{-1} . No well-organized, self-similar solution is visible at the four different times (contrast to Fig. 5 and Fig. 9). At some times the flame resembles the multiple structures in the flamelet regime (compare the lower right with Fig. 2). At others, sizable islands of well-mixed fuel and ash have nearly constant temperature. Some of these (lower left) are almost as large as the integral scale itself. The average width of the flame is still somewhat broader than the integral scale by about a factor of two.

or so. Characteristics of these regions include a carbon mass fraction much less than in the fuel, typically on the rapidly rising part of the energy generation curve in Fig. 12, and temperatures that are a substantial fraction of the ash temperature. The relatively high temperatures are a consequence of the temperature dependent nature of the heat capacity (§ 2.2).

5.4.3. Ledges

The ledges seen in Fig. 13 play an important role in promoting detonation and it is thus worth spending a moment to discuss their credibility. They have not been seen previously in any combustion simulation or experiment. For accessible terrestrial conditions, it is believed that chemical flames in this regime would extinguish (Peters 2000). Numerical exploration of this regime, other than with LEM, has so far been impractical.

Nevertheless, it has long been known that property fields in turbulence exhibit intermittent behavior, including the occurrence of transient well-mixed regions separated by cliffs (sharp property changes). This structure is seen, for instance, in 1D profile data from 3D numer-

ical simulations (Watanabe & Gotoh 2006). A quantitative signature of this structure is the saturation of high-order structure-function exponents, reflecting the dominant contribution of the cliff regions to high-order intermittency statistics (Celani et al. 2000). Measurements by Moisey et al. (2001) show clear evidence of the saturation of the scalar structure-function exponents. LEM structure-function exponents exhibit a somewhat slower roll-off to saturation (Kerstein 1991), suggesting that the prevalence and duration of well-mixed regions in LEM might be lower than actually occurs in turbulence. This is plausible because maps in LEM are statistically independent events, but the eddies that they represent actually occur in bunches because each eddy breakdown is an energy source for subsequent eddy breakdown. This bunching contributes to the intermittency of turbulence.

There is some limited understanding of why turbulence exhibits these properties (Celani et al. 2000). Further clarification would provide insight into a mechanism that appears to play a key role in the timely occurrence of detonations in supernovae.

6. CONDITIONS FOR DETONATION

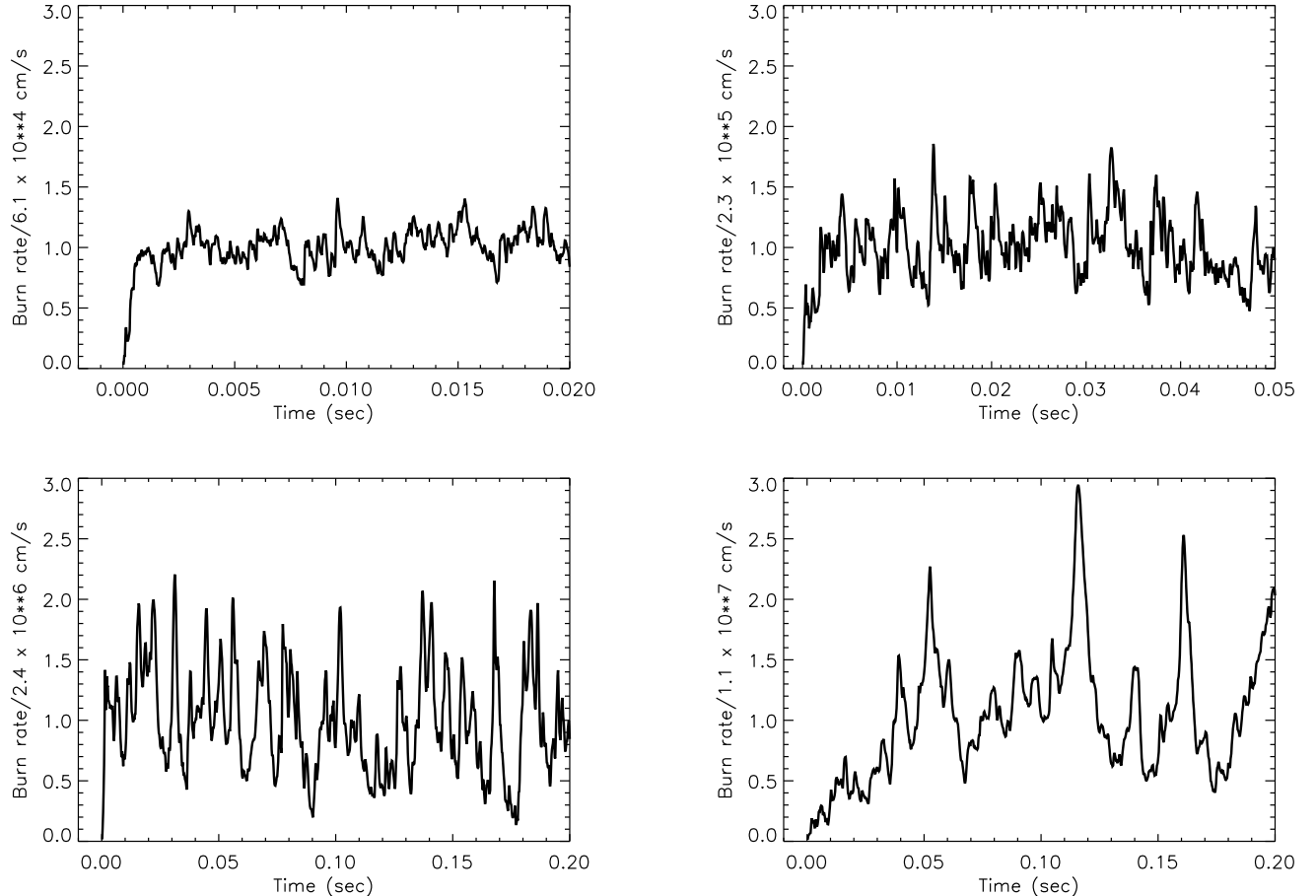


FIG. 11.— Instantaneous flame speed divided by average speed for four different choices of l and v' at a density of 10^7 g cm^{-3} , fuel carbon concentration 50%, and turbulent energy dissipation rate $10^{15} \text{ erg g}^{-1} \text{ s}^{-1}$. The four choices correspond to the four integral scales in Table 2, $l = 120 \text{ cm}$, 960 cm , 614 m , and 4.92 km . For the smallest scale (top left), $l < \lambda = 64 \text{ m}$, and the flame speed (and width) are nearly constant. Going to larger length scales one sees the effect of individual large eddies and unsteady burning. In the last frame (lower right), the flame width and speed are approximately the same as turbulence on the integral scale and large burning rates are seen approximately every l/v' seconds. The speed plotted here is the rate at which a single flame would move into the fuel with a burning rate equivalent to that on the entire grid. The actual burning here actually happens mostly in regions with much smaller carbon concentrations than in the unmixed fuel.

In order that a detonation occur, three conditions must be satisfied. First, some region must burn supersonically. The simplest example would be a hot, isothermal volume in which the nuclear induction time scale was a constant. As the temperature rises, the time scale decreases and for a sufficiently large volume there comes a temperature where the burning time is shorter than the sound crossing time. The pressure will increase in that region faster than expansion can damp its growth and, after a maximum temperature is reached (i.e., the fuel is gone), the region expands at a speed that is somewhat higher than the sound speed in the surrounding medium. In reality, the temperature is never completely isothermal, but, as we shall see, it suffices to burn only some fraction of the fuel within the volume in a sound crossing time. A subset of fluid elements within the volume must have the same temperature to some level of tolerance that depends on their burning time scale. The smaller the fraction, the smaller the overpressure, but sonic expansion nevertheless occurs. The colder matter is an inert dilutant.

Second, the size of the “detonator” must exceed some critical value (Dursi & Timmes 2006; Niemeyer & Woosley 1997). That critical mass is larger if the mass fraction of combustible fuel is small or if the fraction of inert cold matter is large. Because some mixing of ash into the pre-detonation region is unavoidable and because an appreciable amount of carbon must burn to reach temperatures where the time scales start to approach sonic, the critical masses we compute here will be larger than those for mixtures of just carbon and oxygen with a smooth temperature structure. For a given turbulent energy, density must fall to lower values to obtain these larger structures.

Third, and perhaps most subtly, there must exist, in a significant fraction of the mass, preferably at its edge, a nearly sonic phase velocity for the burning (Khokhlov, Oran, & Wheeler 1997; Zeldovich et al. 1985). This is the “shock wave amplification by coherent energy release” (SWACER) mechanism for initiating a detonation in an unconfined medium. One requires an

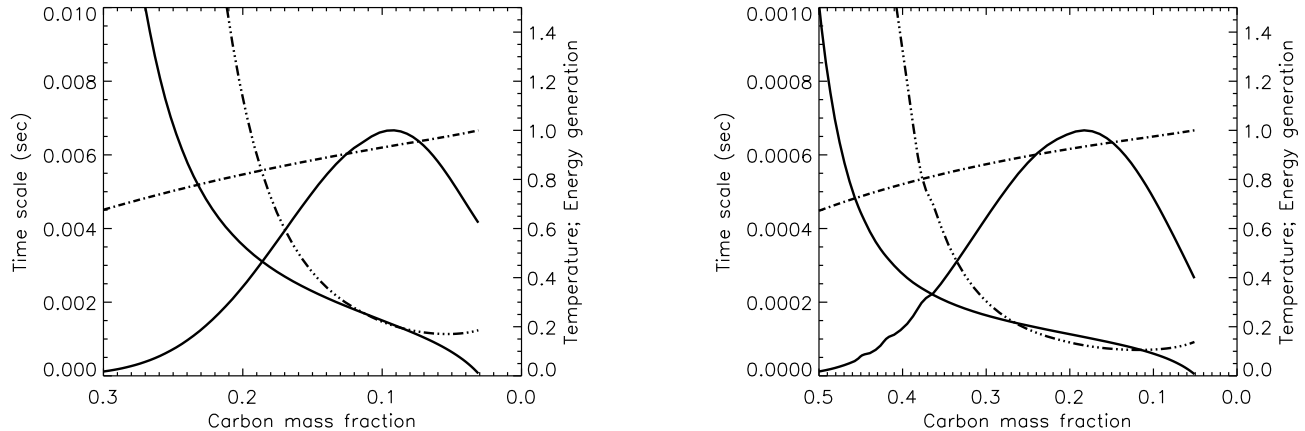


FIG. 12.— Nuclear time scale and energy generation as a function of carbon mass fraction for carbon burning under isobaric conditions. The initial carbon mass fraction in the first frame was 0.50, though only the evolution below 0.30 is shown. Similarly in the second frame the initial carbon mass fraction was 0.75. Solid lines show the induction time scale (the time remaining until most of the carbon is consumed) and the nuclear energy generation rate divided by the maximum value achieved in the evolution. Dashed lines show the nuclear time scale, $[(1/X_{12})(dX_{12}/dt)]^{-1}$, and the temperature divided by the ash temperature. For the 50% carbon run the maximum energy generation and ash temperature were $3.89 \times 10^{19} \text{ erg g}^{-1} \text{ s}^{-1}$, and $2.59 \times 10^9 \text{ K}$. For the 75% run, the corresponding values were $1.29 \times 10^{21} \text{ erg g}^{-1} \text{ s}^{-1}$, and $2.95 \times 10^9 \text{ K}$. The induction time was arbitrarily defined to reach zero when the remaining carbon fraction was 0.03 for the 50% carbon case and 0.05 for the 75% carbon case. Energy released beyond these points is negligible and the time for the carbon to go to precisely zero is arbitrarily long. For high remaining carbon abundance, the induction time scale is much shorter than the instantaneous nuclear time scale because much of the remaining carbon will burn at a higher temperature. Note the relatively small change in induction time over an interesting range of carbon mass fraction, 0.2 to 0.1 (left) and 0.4 to 0.1 (right).

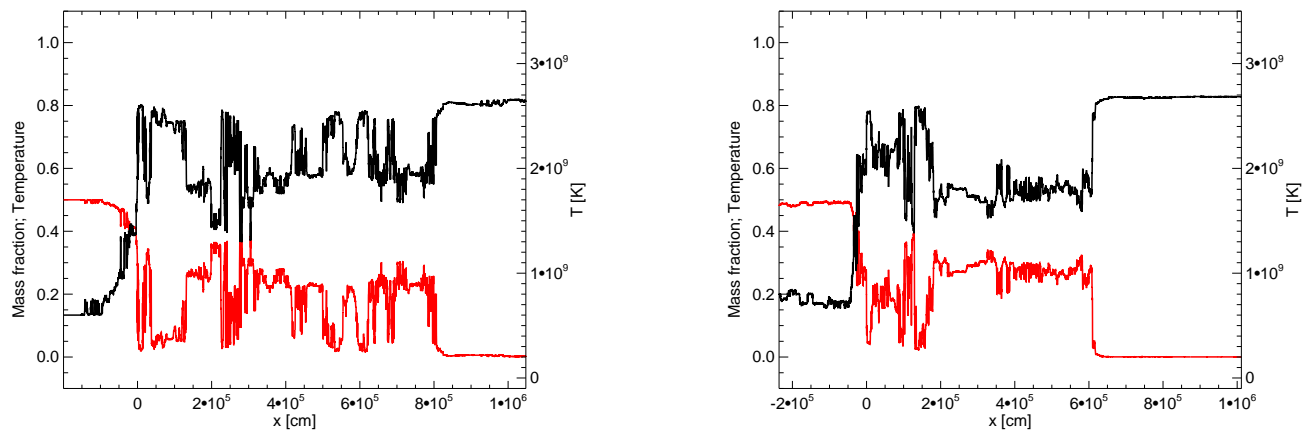


FIG. 13.— A single flame in the stirred flame regime for an integral scale of 4.92 km. The turbulent speed on that scale is 78.9 km s^{-1} and the average flame speed and width are also close to these values. Many complex and folded structures are seen like in Fig. 10, but the above two snapshots show that occasionally quite regular, well-mixed regions of fuel and ash exist. Sometimes several of these structures add together to create a mixed region about as large, or even larger than the integral scale.

appreciable boundary layer where

$$\frac{d\tau_{\text{nuc}}(T)}{dx} \approx (c_{\text{sound}})^{-1}. \quad (16)$$

Two properties of the flame in the SF regime assist in satisfying these three conditions. First is the unsteady nature of the burning (§ 5.4.2). As fuel and ash are mixed, burning may briefly almost go out, only to return with a vengeance after sufficient mixing and slow burning have occurred. This allows the creation of regions that, after some delay comparable to a turnover time, can consume fuel at a rate faster than a single flame moving at the turbulent *rms* speed on the integral scale. Amplifica-

tion factors of three are frequently observed, and larger values are presumably possible in rare instances.

Second, as discussed in § 5.4.3, transient well-mixed structures, ledges, are a frequent occurrence in the SF regime. Turbulence does not always lead to heterogeneity on macroscopic scales. These mixed regions have relatively constant induction time and they are at least occasionally bounded by regions in which the temperature decreases (and fuel concentration increases) fairly smoothly. The characteristic size of these regions is approximately λ , which increases with decreasing density. As a result, the ratio of mixing time to sound crossing

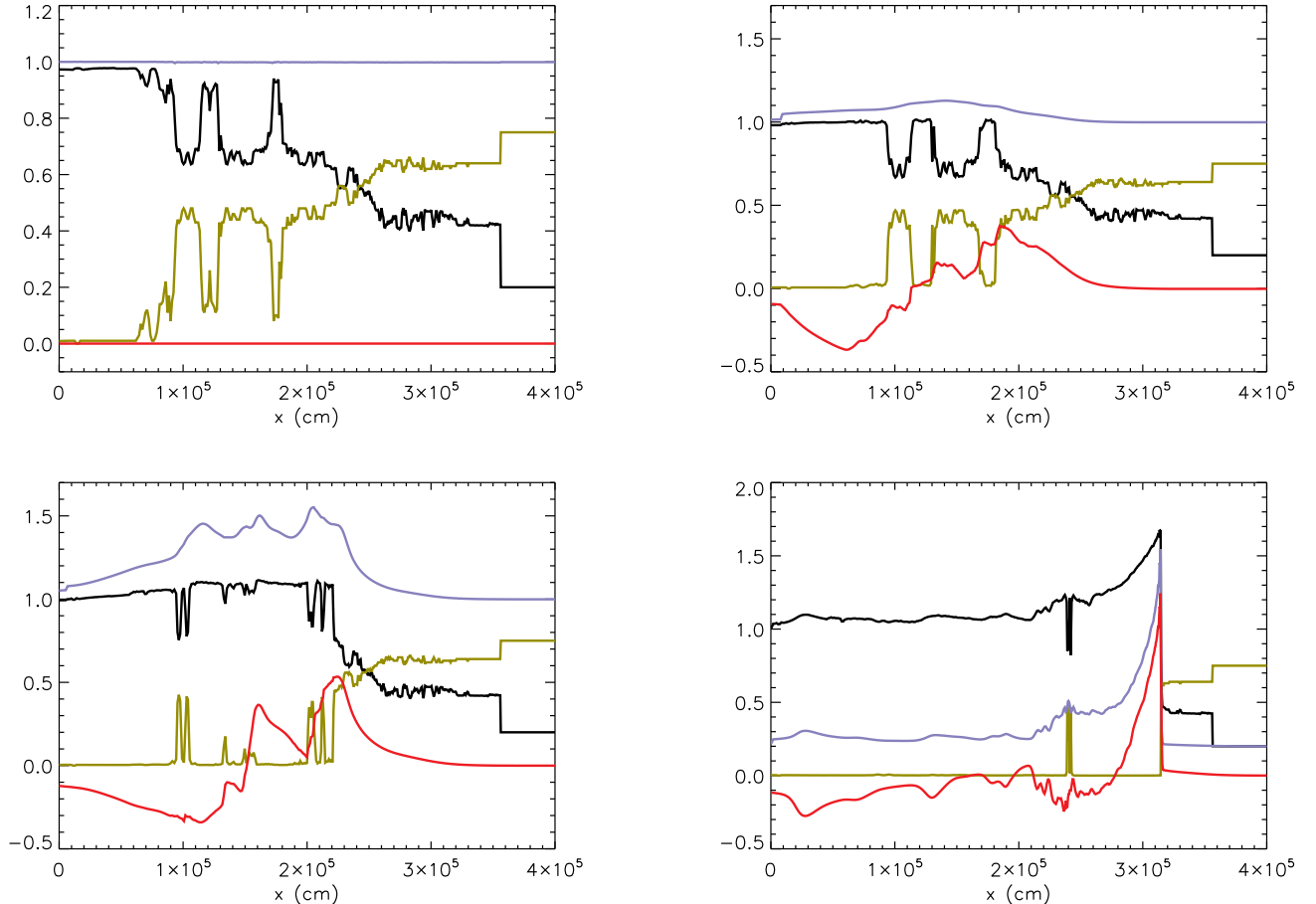


FIG. 14.— The birth of a detonation. A sample mixture calculated using LEM for a density $1.0 \times 10^7 \text{ g cm}^{-3}$, $v' = 500 \text{ km s}^{-1}$, and $L = 10 \text{ km}$ was mapped into a compressible hydrodynamics code and its subsequent evolution was followed. The time selected was characterized by a very subsonic flame speed but temperature gradients that looked “interesting”. Following the remap, which preserved distance scale, ash was on the left and fuel on the right. A detonation developed that, barring large barriers of ash, would explode the whole star (see text). Shown in the plot are carbon mass fraction (gold), pressure (blue), temperature (black), and velocity (red) at four different times - 0, 0.15, 0.30, and 0.43 ms after the mapping. The velocity has been divided by 500 km s^{-1} in frames 1 and 2, 2000 km s^{-1} in frame 3 and 5000 km s^{-1} in frame 4. The pressure has been scaled by the background value, $9.08 \times 10^{23} \text{ dyne}$, in frames 1, 2, and 3, and by an additional factor of 5 in frame 4. The temperature has been divided by $3.0 \times 10^9 \text{ K}$.

time decreases, since

$$\frac{\tau_t}{\tau_{\text{sonic}}} \propto \frac{\lambda^{2/3}}{\lambda} = \lambda^{-1/3}, \quad (17)$$

and this helps detonation happen. However, as the density decreases, the critical size required to initiate a detonation also increases dramatically (Niemeyer & Woosley 1997; Woosley 2007), so mixing a smaller region at higher density may, in some cases, be better than a larger one at low density. Detonation may occur before the characteristic size of the mixed region becomes equal to the integral scale.

Another important point favoring detonation is that once burning starts to happen on a time scale approaching sonic, it no longer occurs at constant pressure. The pressure rises with respect to the surrounding fuel and is not immediately relieved by expansion. At constant volume, a given amount of carbon burning raises the temperature more, thus appreciably shortening the time scale for additional burning. That is, for the relevant

conditions, the heat capacity at constant pressure is appreciably larger than the heat capacity at constant volume. The final temperature from burning all the fuel is also higher.

6.1. Detonation Observed for a Mixture Calculated Using LEM

In order to verify that some of the mixed regions calculated using LEM would actually detonate, the burning of select mixtures was followed using the compressible hydrodynamics code, Kepler (Weaver, Zimmerman, & Woosley 1978; Woosley et al. 2002, Fig. 14). The composition and temperature structure were taken from an LEM simulation of flame-turbulence interaction at a density of $1.0 \times 10^7 \text{ g cm}^{-3}$ for a characteristic turbulent speed of 500 km s^{-1} on an integral scale of 10 km (Table 2). Carbon had a mass fraction of 0.75 in the fuel. Use of 65536 zones gave a characteristic Reynolds number of 80,000 and a resolution not achievable in a multi-dimensional simulation

on this length scale. The LEM calculation was run for 0.10 s, or 5 eddy turnover times on the integral scale, during which 40 dumps were created at equal time intervals. Visual inspection isolated several cases for further study. One of these was dump number 28, made 70 ms after the beginning of the run. The overall burning rate at this time was not particularly high, corresponding to an effective speed of only 250 km s^{-1} . However, most of the energy generation was occurring in regions where the carbon mass fraction was already low (Fig. 14), so the local *rate* of pressure increase was quite large, even though the integrated total change in pressure in the end was small.

Kepler, frequently used for studying stars and supernova explosions, is an implicit 1D hydrodynamics code with a spherical Lagrangian mesh. In order to simulate a problem with approximately plane parallel geometry, the 4 km of interest was mapped on top of a sphere of pure ash (mostly magnesium and silicon) with a radius 10 km so that LEM zones of constant thickness had approximately constant mass and thickness in Kepler. In the figure, that 10 km has been subtracted off of the x-coordinate. The overall thickness in km of the region of interest was the same in the Kepler study as in the LEM calculation. The temperature was by no means isothermal in this region. In fact, an isothermal runaway would not have initiated a detonation here, even if the burning were supersonic. However, several key elements favoring detonation were in place. First, there were some regions where the temperature was already high because of previous mixing and burning. The rate of carbon burning was quite high in these regions with a peak energy generation rate near $10^{21} \text{ erg g s}^{-1}$. These were embedded in an extended region with $X_{12} \approx 0.4$ that was already quite warm due to mixing. Finally that mixture lay at the base of a region where the carbon mass fraction increased steadily, if somewhat noisily, in an outwardly direction. It is important to emphasize that this was the result of an LEM calculation, and not an artificial construct.

During the first phase, the “initiator” burned rapidly producing an overpressure in the surrounding zones of about 10 - 15%. This increase was sufficient to cause the warm material to burn faster, on a roughly sonic time scale. Their expansion then compressed and ignited material at successively higher carbon mass fractions in the gradient. While weak at first, the detonation strengthened and by the last frame shown was strong enough that its permanent propagation was guaranteed. It was followed until it left the grid. Among the interesting implications here is that a region need not be highly isothermal, nor need all of it initially burn on a supersonic time scale to provoke a detonation, though near sonic speeds are needed. A pile up of strong acoustic pulses at around 2.3 km initiates the runaway.

6.2. Active Turbulent Combustion

Almost as interesting were the many other sample mixtures in this and other runs that, when mapped into Kepler, did *not* detonate. Instead, the irregular burning that is characteristic of combustion in the SF regime produces strong pressure waves. A particularly strong pulse occurs roughly every turnover time on the integral scale because these big mixing events trigger a lot of burning.

An example from the same run that produced the detonation in Fig. 14 is shown about one turnover time later (dump 39 at 95 ms) in Fig. 15. This time the burning did not produce a detonation, but substantial burning still occurred on less than a sonic time scale for the 4 km shown (the sound crossing time for this region is about 1 ms). This burning produced a strong pulse that sent matter moving inwards and outwards at $\sim 600 \text{ km s}^{-1}$, about the same value as assumed for turbulence on an integral scale of 10 km in the study.

In three dimensions, these pulses would be quasi-spherical and would occur all over the surface where burning and mixing are going on. Collisions between the fronts would pump additional energy into turbulence on a scale comparable to the width of the burning region, i.e., the integral scale, or about 10 km. As noted, the velocities in these pulses are frequently larger than expected from the assumed turbulent energy on that length scale. As discussed by Kerstein (1996); Niemeyer & Woosley (1997), this sets the stage for a potential runaway. More turbulence leads to increased mixing which leads to more violent irregular burning, which creates more turbulence. The culmination of this runaway could be a detonation.

7. CONCLUSIONS

Three regimes of turbulent flame propagation relevant to nuclear burning in a Type Ia supernova have been explored. At high density, for Karlovitz numbers less than about one, burning occurs in multiply folded laminar flames. The overall progress of burning is governed by the turbulent energy and has a speed that is independent of the laminar speed. A similar description of “laminar flame brushes” has been given many times in the literature, but this is the first time it has been simulated in a supernova (e.g., Fig. 2).

The average number of flamelets in the flame brush is U_L/S_{lam} , and initially is not large. Because of this, there will be considerable variation in the burning rate. We estimate such variations to be as large as a factor of three. However, detonation does not happen so early because the turbulent speed then is very subsonic and the individual flamelets are thin. Later, the number of flamelets becomes very large, reaching hundreds or even thousands, and variations in the overall burning rate are much smaller. Detonation remains impossible in the flamelet regime. No critical mass of hot fuel can be obtained.

As the Karlovitz number increases above about 10, hot ash and cold fuel can be mixed for the first time and detonation is, in principle, possible. Two cases of turbulent burning were explored corresponding to the well-stirred reactor (WSR; $Da < 1$, § 5.3) and stirred flames (SF; $Da > 1$; § 5.4). In the WSR regime, turbulent diffusion substitutes for heat diffusion and turbulently broadened flames result. These flames can be much larger than the integral scale. Because the integral scale in a supernova is so large, this limiting case is probably never fully realized, but is amenable to numerical simulation (Aspden et al. 2008). We normalized an uncertain constant in the LEM calculation, C , (§ 3.1) to those simulations. In the stirred flame regime, one again has something like a flame brush, but with turbulently broadened structures substituting for the individual flamelets in the flamelet regime. The structure of burning here is com-

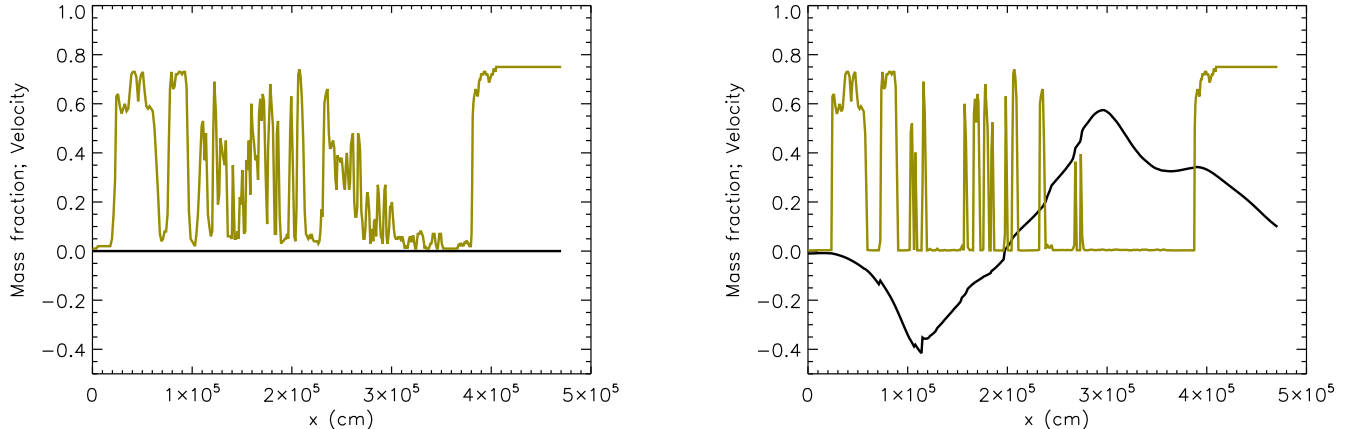


FIG. 15.— Development of a small scale explosion within a flame front in the WSR regime. The highly variable gold line is the carbon mass fraction. The dark line that is initially zero is the velocity. The velocity scale is in units of 1000 km s^{-1} . Unlike in Fig. 14, the rapid burning of a mixed region does not initiate a detonation here, but it does produce a strong subsonic pulse. These may be very common events and would be a mechanism for adding turbulent energy at the flame scale. The two edits here are from the same run that produced the detonation in Fig. 14 sampled $3.9 \times 10^{-4} \text{ s}$ apart.

plex and highly variable. Because the burning time scale is very temperature sensitive, it is possible to mix large regions of “warm” fuel and ash in which are embedded smaller nuggets on the verge of explosion. Mixed regions of nearly constant temperature are sometimes observed (Fig. 13, § 5.4.3).

Spontaneous detonation can happen in the SF regime (Fig. 14, § 6.1). It does not require complete mixing on the integral scale, and hence $Da \approx 1$ as discussed in Woosley (2007), but is favored by values of Da that are not large. The necessary conditions occur infrequently and require a favorable confluence of several mixed regions including: a) some region, perhaps not large and with a low mass fraction of carbon, where the burning occurs sufficiently rapidly to increase the pressure by a small fraction supersonically; and b) an extended region where the carbon mass fraction rises gradually and the temperature falls slowly. Neither region need be particularly homogeneous as long as some part of the composition burns supersonically for condition a) and there are neither large barriers of ash or abrupt, sustained increases in carbon mass fraction for condition b).

In general, the production of these situations require turbulent speeds that are already a considerable fraction of sonic, certainly within 10% and probably 20%. Overall the progress of burning in the SF regime varies frequently by a factor of three up and down, and rare excursions to larger values probably also occur due to intermittency (Pan et al. 2008). We also find that appreciable turbulence can be put into the burning region on a scale comparable to the integral scale by small subsonic explosions of mixtures that fail to detonate (§ 6.2, Fig. 15). Before the big bang in these stars, there is a lot of thunder. Though we have not demonstrated it here, we speculate that this energy input may exceed that put in at the large scale by the flame instabilities. If so, there is the possibility of a turbulent runaway in which mixing pumps energy into turbulence which in turn causes accelerated mixing (Kerstein 1996). The endpoint would

be detonation.

These necessary conditions for detonation are summarized in Fig. 16. Detonation is estimated to occur for a reasonable range of turbulent energies in the nearly horizontal band between the lines $Da = 10$ and $Da = 100$. It must be acknowledged that this figure is very approximate because the nuclear time scale (and hence Damköhler number) are poorly determined. The effective nuclear time scale in Da is probably longer than in Table 3 and intermittency essentially raises the effective turbulent speed making detonation possible at a higher density. This is why the conditions $Da = 10 - 100$ in Fig. 16 are probably more favored than say 1 to 10. Above $Da = 100$, the mixed regions may be too small to initiate a detonation.

Three-dimensional simulations by Röpke (2007) show that the necessary degree of turbulence for detonation, roughly $u' = 500 \text{ km s}^{-1}$, is realized in the full star models.

We also find some dependence of the detonation conditions on initial carbon mass fraction (see also Woosley 2007). For lower carbon mass fractions, Damköhler numbers of order 10 are reached at a higher density. If detonation does occur at a higher density, the explosion makes more ^{56}Ni and a brighter supernova. However, detonation depends on achieving a significant overpressure on a sonic time scale. By the time that carbon-poor fuel carbon reaches a temperature where it burns rapidly (Fig. 12), the remaining burning produces too small an overpressure. Detonating carbon-rich fuel is, in this sense, easier (see also Umeda et al. 1999a,b). It is important to note that the relevant location for detonation is probably in the outer layers where the density first declines below 10^7 g cm^{-3} at the flame front, not near the center. The carbon abundance is higher in these outer layers.

All in all, our results are supportive of the hypothesis that some, perhaps even all Chandrasekhar mass white dwarfs explode by a delayed detonation that oc-

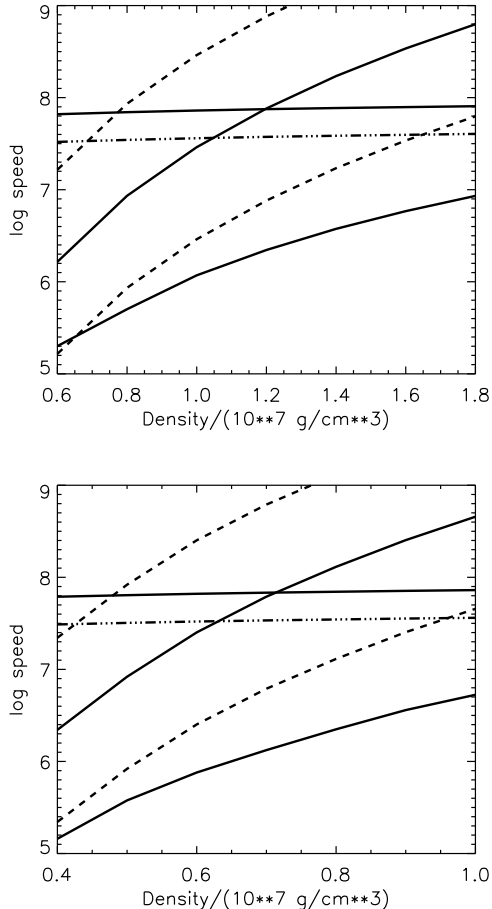


FIG. 16.— Speeds required on an integral scale of 10 km to establish the necessary conditions for detonation. The first panel is for an initial carbon mass fraction of 50%; the second, for 75%. The solid line that increases rapidly from left to right is the condition $Da = 10$ and the two dashed line parallel to it are $Da = 1$ (upper) and 100 (lower). The nearly horizontal solid line is the sound speed divided by 5 and the dash-dotted line beneath is the sound speed divided by 10. The lowest solid line is the condition $Ka = 10$. Scaling to other values is given in the text. In order to detonate the speed on the integral scale must be greater than that given by $Ka = 10$ and in the vicinity of $Da = 10$. It is also necessary that the turbulent speed be at least $1/10$ the sound speed and, better still, $1/5$ the sound speed, but turbulent speeds above 20% sonic may not be achieved in the star. Thus detonation for the assumed conditions and a carbon mass fraction of 0.5 probably occurs in the band between 0.8 and $1.6 \times 10^7 \text{ g cm}^{-3}$. For 75% carbon, the likely density range is 0.5 to $1.0 \times 10^7 \text{ g cm}^{-3}$.

curs shortly after the burning enters the SF regime. This would then make the location and number of detonation points, along with the ignition conditions (Kuhlen et al. 2006), the principal determining factors in the intrinsic properties of a Type Ia supernova.

Several avenues for future investigation are opened up by this work. First, our results hinge on the calibration of the 1D LEM model to direct 3D simulation (Aspden et al. 2008). The 3D study used for normalization here was carried out in the WSR regime, but the results (e.g., the constant C) were assumed to be valid in the SF regime. Given the subgrid model developed here, it should be possible to carry out equivalent 3D studies for the SF regime ($Da \gg 1$).

The results for detonation (§ 6.1) and active turbulent combustion (§ 6.2) were obtained by mapping results from LEM using a linear grid into a 1D compressible hydro-code with spherical coordinates. It would be greatly preferable to see both the mixing and the strong pressure waves in the same, preferably 3D study. Because of the range in length scales, the need for a large effective Reynolds number, and the rare, transient nature of the phenomena, this will require a very major investment of computational resources, but should be practical in the near future.

Ultimately, of course, one would want to see these results applied to full scale models of the supernova and its light curve.

The authors gratefully acknowledges helpful conversations on the subject of the paper with Andy Aspden, John Bell, and Martin Lisewski. This research has been supported by the NASA Theory Program (NNG05GG08G) and the DOE SciDAC Program (DE-FC02-06ER41438). Work at Sandia was supported by the US Department of Energy, Office of Basic Energy Sciences, Division of Chemical Sciences, Geosciences and Biosciences. Sandia is a multiprogram laboratory operated by Sandia Corporation, a Lockheed Martin Company, for the US Department of Energy under contract DE-AC04-94AL85000.

A. LEM FLAME SPEED IN THE FLAMELET REGIME

Properties of the triplet map imply a simple, exact expression for the turbulent burning velocity v_{turb} in terms of the LEM parameters D_{turb} (turbulent diffusivity) and L (largest allowed map size) under the conditions $v_{\text{turb}} \gg S_{\text{lam}}$ (here assuming the flamelet regime) and $D_{\text{turb}} \gg \nu/\rho$ (implying $Re \gg 1$). On the LEM domain (coordinate x), assume fuel on the right and ash on the left, so the flame advances rightward (direction of increasing x). v_{turb} is evaluated by tracking the forward progress of the rightmost (forwardmost) ash location. The only mechanism affecting this location, denoted r , is the triplet map because small S_{lam} implies that the contribution of laminar burning is negligible.

Any triplet map containing r maps r to three locations, the rightmost of which, denoted r' , exceeds r . Specifically, if the map interval is $[x_1, x_2]$, then $r' = x_2 - \frac{1}{3}(x_2 - r)$, i.e., the distance from r' to x_2 is one third of the pre-map distance. The advancement of the rightmost ash location is therefore $r' - r = \frac{2}{3}(x_2 - r)$.

Suppose that the interval $[x_1, x_2]$ is chosen arbitrarily. If it contains r , then r is equally likely to be anywhere within the interval, and hence is uniformly distributed in the interval. The advancement is therefore averaged over r values

in the interval. Because the advancement is linear in r , this implies that the average value $(x_1 + x_2)/2$ is substituted for r , giving the average advancement $\langle r' - r \rangle = \frac{1}{3}(x_2 - x_1) = \frac{1}{3}l$, where l is the map size.

Suppose that all maps were the same size l and denote the frequency of maps containing a given location as ϕ . Then the average rate v_{turb} of advancement of r is ϕ times the average advancement of r per map, giving $v_{\text{turb}} = \frac{1}{3}\phi l$.

ϕ can be expressed in terms of D_{turb} . From random walk theory, D_{turb} is one-half of the frequency of events that displace a point times the mean-square displacement per event. The mean-square displacement induced by a size- l triplet map is $\frac{4}{27}l^2$ citepart5, so $D_{\text{turb}} = \frac{2}{27}\phi l^2$, giving $\phi = \frac{27}{2}D_{\text{turb}}/l^2$ and thus $v_{\text{turb}} = \frac{9}{2}D_{\text{turb}}/l$. This illustrates the analysis but is not the case of interest because inertial-range turbulence is represented in LEM by a distribution of map sizes l .

As explained in Kerstein (1991), in LEM the map size distribution is $f(l) = Al^{-8/3}$ for l in the range $[\eta, L]$, where A is a normalization factor. The total frequency of maps of all sizes per unit domain length is denoted Λ . The frequency of maps in the size range $[l, l + dl]$ that contain a given point is then $\Lambda l f(l) dl$, so $D_{\text{turb}} = \frac{2}{27}\Lambda \int l^3 f(l) dl = \frac{1}{18}\Lambda A(L^{4/3} - \eta^{4/3})$. For high Re, the η term is negligible and is dropped, giving $D_{\text{turb}} = \frac{1}{18}\Lambda AL^{4/3}$.

To obtain v_{turb} , the average advancement $\frac{1}{3}l$ for map size l is multiplied by $\Lambda l f(l) dl$ and integrated over l to obtain (ignoring the η term) $v_{\text{turb}} = \Lambda AL^{1/3}$. In terms of D_{turb} , the result $v_{\text{turb}} = 18D_{\text{turb}}/L$ is obtained. The numerical factor is four times larger than if all maps were of size L . A heuristic interpretation of this result is that the typical map size from a flame propagation viewpoint is $L/4$ when $f(l)$ is based on inertial-range scaling.

REFERENCES

- Aspden, A. J., Bell, J. B., Day, M. S., Woosley, S. E., & Zingale, M. 2008, submitted to ApJ
- Bell, J. B., Day, M. S., Rendleman, C. A., Woosley, S. E., & Zingale, M. 2004, ApJ, 606, 1029
- Bell, J. B., Day, M. S., Rendleman, C. A., Woosley, S. E., & Zingale, M. 2004, ApJ, 608, 883
- Bildsten, L., & Hall, D. M. 2001, ApJ, 549, L219
- Celani, A., Lanotte, A., Mazzino, A. & Vergassola, M. 2000, Phys. Rev. Lett., 84, 2385
- Damköhler, G. 1940, Z. Elektrochem, 46, 601
- Dursi, L. J., & Timmes, F. X. 2006, ApJ, 641, 1071
- Hansen, J.-P., McDonald, I. R., & Pollock, E. L. 1975, Phys. Rev. A, 11, 1025
- Hillebrandt, W., & Niemeyer J. 2000, ARAA, 38, 191b
- Kerstein, A. 1991, J. Fluid Mech., 231, 361
- Kerstein, A. 1996, Combust. Sci. Tech., 118, 189
- Kerstein, A. 2001, Phys. Rev. E., 64, 066306
- Khokhlov, A., Oran, E. S., & Wheeler, J. C. 1997, ApJ, 478, 678
- Kuhlen, M., Woosley, S. E., & Glatzmaier, G. A. 2006, ApJ, 640, 407
- Landau, L., & Lifshitz, F. M. 1959, Course in Theoretical Physics, Vol. 6. Fluid Mechanics (Oxford:Pergamon)
- Lisewski, A. M., Hillebrandt, W., & Woosley, S. E. 2000, ApJ, 538, 831
- Moisy, F., Willaime, H., Andersen, J. S., & Tabeling, P. 2001, Phys. Rev. Lett., 86, 4827
- Nandkumar, R., & Pethick, C. J. 1984, MNRAS, 209, 511
- Niemeyer, J. C. 1995, PhD Thesis, MPA, Munich, Germany: Technical University
- Niemeyer, J. C., & Hillebrandt, W. 1995, ApJ, 452, 779
- Niemeyer, J. C., & Woosley, S. E. 1997, ApJ, 475, 740
- Niemeyer, J. C., & Kerstein, A. R. 1997, New Astronomy, 2, 239
- Pan, L., Wheeler, J. C., & Scalo, J. 2008, ApJ, 681, 470
- Peters, N. 1986, Proc. Combust. Inst., 21, 1231
- Peters, N. 2000, Turbulent Combustion, by Norbert Peters, pp. 320. ISBN 0521660823. Cambridge, UK: Cambridge University Press, August, 2000
- Röpke, F. K., Hillebrandt, W., & Niemeyer, J. C. 2004, A&A, 420, 411
- Röpke, F. 2007, ApJ, 668, 1103
- Schmidt, W., Niemeyer, J. C., & Hillebrandt, W. 2006, A&A, 450, 265
- Schmidt, W., Niemeyer, J. C., Hillebrandt, W., Röpke, F. K. 2006, A&A, 450, 283
- Smith, T. M. & Menon, S. 1997, Combust. Sci. Tech., 128, 99
- Timmes, F. X., & Woosley, S. E. 1992, ApJ, 396, 649
- Timmes, F. X. 2000, ApJ, 528, 913 see also http://cococubed.asu.edu/code_pages/eos.shtml
- Timmes, F. X., & Swesty, F. D. 2000, ApJS, 126, 501, see also http://cococubed.asu.edu/code_pages/eos.shtml
- Timmes, F. X., Hoffman, R. D., & Woosley, S. E. 2000, ApJS, 129, 377
- Umeda, H., Nomoto, K., Kobayashi, C., Hachisu, I., & Kato, M. 1999a, ApJ, 522, L43
- Umeda, H., Nomoto, K., Yamaoka, H., & Wanajo, S. 1999b, ApJ, 513, 861
- Watanabe, T., & Gotoh, T. 2006 Phys. Fluids, 18, 058105
- Weaver, T. A., Zimmerman, G. B., & Woosley, S. E. 1978, ApJ, 225, 1021
- Woosley, S. E., Heger, A., & Weaver, T. A. 2002, Reviews of Modern Physics, 74, 1015
- Woosley, S. E., Wunsch, S., & Kuhlen, M. 2004, ApJ, 607, 921
- Woosley, S. E. 2007, ApJ, 668, 1109
- Zeldovich, Ya. B., Barenblatt, G. I., Librovich, V. B., & Makhviladze, G. M. 1985, *The Mathematical Theory of Combustion and Explosions*, Consultants Bureau, Plenum Press.

TABLE 1. PROPERTIES OF LAMINAR FLAMES

X_{12}	ρ (10^7 g cm $^{-3}$)	S_{lam} (cm/s)	$\delta_{\text{lam}}(\epsilon)$ (cm)	$\delta_{\text{lam}}(T)$ (cm)	$\delta_{\text{lam}}(C)$ (cm)
0.50	0.6	8.62(2)	11.7	15.6	19.3
0.50	0.8	1.77(3)	4.35	6.01	7.03
0.50	1.0	3.23(3)	2.08	3.12	3.32
0.50	1.2	4.99(3)	1.15	1.78	1.82
0.50	1.4	7.19(3)	0.70	1.14	1.10
0.50	1.6	9.66(3)	0.45	0.76	0.72
0.50	1.8	1.26(4)	0.31	0.54	0.50
0.50	2.0	1.58(4)	0.22	0.40	0.36
0.50	2.5	2.47(4)	0.12	0.23	0.19
0.50	3.0	3.54(4)	0.067	0.14	0.11
0.50	3.5	4.66(4)	0.041	0.090	0.065
0.75	0.3	1.73(2)	172	157	325
0.75	0.4	8.65(2)	21.4	22.4	40.0
0.75	0.5	1.74(3)	9.80	11.4	17.7
0.75	0.6	2.80(3)	5.02	6.12	8.94
0.75	0.7	4.10(3)	2.94	3.52	5.29
0.75	0.8	5.86(3)	1.80	2.27	3.21
0.75	0.9	8.39(3)	1.25	1.73	2.20
0.75	1.0	1.08(4)	0.85	1.21	1.49
0.75	1.2	1.70(4)	0.43	0.66	0.77
0.75	1.4	2.37(4)	0.25	0.40	0.45

TABLE 2. FLAME PROPERTIES AT $\rho = 1.0 \times 10^7 \text{ G CM}^{-3}$

X_{12}	l (cm)	U_L (km/s)	Zones	Δx (cm)	Transport	v_f (km/s)	$\delta_f(\epsilon)$ cm	$\delta_f(T)$ cm
0.50	-	0	2048	0.0244	rad	0.0323	2.1	3.1
0.50	-	0	256	0.196	rad	0.0314	2.1	3.1
0.50	15	2.47	2048	0.244	rad.	0.149	40	70
0.50	15	2.47	2048	0.244	SG	0.156	40	70
0.50	120	4.93	2048	0.977	SG	0.61	160	300
0.50	960	9.86	2048	9.77	SG	2.3	~700	~1200
0.50	960	9.86	16384	1.22	SG	2.3	~700	~1200
0.50	7680	19.7	8192	9.77	SG	8.2	fluc.	fluc.
0.50	6.14(4)	39.4	32768	9.16	SG	26	fluc.	fluc.
0.50	4.92(5)	78.9	65536	49.9	SG	110	fluc.	fluc.
0.50	3.93(6)	158	65536	360	SG	280	fluc.	fluc.
0.50	3.93(6)	340	65536	360	SG	440 - 470?	fluc.	fluc.
0.75	-	0	2048	0.0391	rad	0.113	0.85	1.2
0.75	10	2.16	2048	0.0977	rad	0.415	10	20
0.75	40	3.42	4096	0.0977	rad	0.922	~25	~60
0.75	80	4.31	8192	0.0977	rad	1.46	~40	~90
0.75	80	4.31	8192	0.0977	SG	1.54	~40	~90
0.75	320	6.84	32768	0.0977	SG	3.2	fluc.	fluc.
0.75	2560	13.7	32768	0.391	SG	12	fluc.	fluc.
0.75	2.05(4)	27.4	32768	3.05	SG	40	fluc.	fluc.
0.75	1.00(4)	215	32768	2.50	SG	96	fluc.	fluc.
0.75	1.00(6)	500	32768	152	SG	1020	fluc.	fluc.
0.75	1.00(6)	500	65536	76.3	SG	870	fluc.	fluc.

TABLE 3. CHARACTERISTIC SCALES IN THE WSR AND ST REGIMES FOR $U_L = 100 \text{ km s}^{-1}$ AND $L = 10 \text{ km}$

X_{12}	ρ (10^7 g cm^{-3})	τ_{nuc} (sec)	λ (cm)	d (cm)	Ka
0.50	0.6	6.1(-2)	4.7(5)	1.0(2)	3.5(3)
0.50	0.8	1.2(-2)	4.0(4)	1.8(2)	8.9(2)
0.50	1.0	3.5(-3)	6.4(3)	3.2(2)	2.5(2)
0.50	1.2	1.3(-3)	1.5(3)	5.0(2)	9.6(1)
0.50	1.4	5.8(-4)	4.5(2)	7.2(2)	4.3(1)
0.50	1.6	2.9(-4)	1.6(2)	9.7(2)	2.2(1)
0.50	1.8	1.6(-4)	6.4(1)	1.3(3)	1.3(1)
0.50	2.0	9.5(-5)	2.9(1)	1.6(3)	7.5(0)
0.50	2.5	3.2(-5)	5.7(0)	2.5(3)	2.8(0)
0.50	3.0	1.3(-5)	1.5(0)	3.5(3)	1.2(0)
0.50	3.5	6.4(-6)	5.1(-1)	4.7(3)	6.4(-1)
0.75	0.3	3.6(-1)	6.8(6)	1.7(1)	1.8(5)
0.75	0.4	6.0(-2)	4.6(5)	8.7(1)	5.8(3)
0.75	0.5	1.6(-2)	6.4(4)	1.7(2)	1.4(3)
0.75	0.6	5.3(-3)	1.2(4)	2.8(2)	4.8(2)
0.75	0.7	2.1(-3)	3.0(3)	4.1(2)	2.1(2)
0.75	0.8	1.0(-3)	9.9(2)	5.9(2)	9.5(1)
0.75	0.9	5.0(-4)	3.5(2)	8.4(2)	4.6(1)
0.75	1.0	2.8(-4)	1.4(2)	1.1(3)	2.6(1)
0.75	1.2	1.0(-4)	3.3(1)	1.7(3)	9.4(0)
0.75	1.4	4.5(-5)	9.6(0)	2.4(3)	4.3(0)